Characterisation of mafic enclaves in the erupted products of Soufrière Hills Volcano, Montserrat 2009-2010

Melissa Plail[1*], Jenni Barclay[1], Madeleine C. S. Humphreys[2], Marie Edmonds[3], Richard A. Herd[1] & Thomas Christopher[4]

[1] School of Environmental Sciences, University of East Anglia, Norwich, NR4 7TJ, UK

[2] Department of Earth Sciences, University of Oxford, South Parks Road, Oxford, OX1 3AN, UK

[3] Department of Earth Sciences, University of Cambridge, Downing Street, Cambridge, CB2 3EQ, UK

[4] Montserrat Volcano Observatory, Flemings, Montserrat, West Indies

*Corresponding author: m.plail@uea.ac.uk

Abstract

Lavas from the current eruption of the Soufrière Hills Volcano, Montserrat exhibit evidence for magma mingling, related to the intrusion of mafic magma at depth. We present detailed field, petrological, textural and geochemical descriptions of mafic enclaves in andesite erupted during 2009-2010, and subdivide the enclaves into three distinct types. Type A are mafic, glassy with chilled margins and few inherited phenocrysts. Type B are more evolved with high inherited phenocryst contents and little glass, and are interpreted as significantly hybridised. Type C are composite, with a mafic interior (type A) and a hybrid exterior (type B). All enclaves define tight linear compositional trends, interpreted as mixing between a mafic end-member (type A) and host andesite. Enclave glasses are rhyolitic, owing to extensive crystallisation during quenching. Type A quench crystallisation is driven by rapid thermal equilibration during injection into the andesite. Conversely, type B enclaves form in a hybridised melt layer, which ponded near the base of the chamber and cooled more slowly. Vesiculation near the mafic-silicic interface resulted in disruption of the hybridised layer and the formation of the Type B enclaves. The composite enclaves represent an interface between types A and B, suggesting multiple episodes of mafic injection.

Number of words: 8964

Number of tables: 6

Number of figures: 12

Number of references: 61

Abbreviated title: Mafic enclaves at SHV

The process of magma mingling, where two or more magmas mix incompletely during magma storage in the crust, is commonly associated with arc volcanism (*e.g.* Pallister *et al.* 1992; Clynne 1999) and results in the formation of banded pumice and magmatic mafic enclaves (*e.g.* Bacon 1986; Clynne 1999; Browne *et al.* 2006b; Martin *et al.* 2006b). More complete mixing of magmas is inhibited by large contrasts in viscosity and density, reflecting differences in temperature, composition and crystallinity, and the relative proportions of the incoming and host magmas (Eichelberger 1980; Bacon 1986; Sparks & Marshall 1986). The textures of enclaves form in response to the local crystallisation conditions, and can yield information about the mingling processes or the dynamics of the intruding magma. For example, the presence of a diktytaxitic framework composed of elongate quench crystals and chilled enclave margins indicates rapid undercooling (Bacon 1986). Enclaves without chilled margins and more tabular framework crystals can indicate that they were predominantly crystallised prior to incorporation into the host magma (solid-liquid mingling) (*e.g.* Eichelberger 1980; Coombs *et al.* 2002). Therefore these enclaves may represent the remnants of a fragmented vesiculated mafic layer from the silicic-mafic interface (Eichelberger 1980; Thomas & Tait 1997; Martin *et al.* 2006a). Formation of a discrete layer of mafic magma is typically thought to be a product of slow and small volume material injection, where viscosity, density and temperature contrasts between the two magmas are strong (Sparks & Marshall 1986). In contrast, enclaves that predominantly crystallised after incorporation into the host reflect direct injection of intruding magma into the host and therefore a more dynamic mingling relationship (Bacon 1986; Sparks & Marshall 1986; Clynne 1999). For example, at Unzen, Japan, Browne *et al*. (2006a) use textural differences to infer whether enclaves sampled represent the slower cooling of the centre of an intrusion or the silicic-mafic interface where there is a high degree of undercooling.

As well as mafic enclaves, disequilibrium textures within both the host rock and enclaves can also be used to track mingling dynamics. Examples of these disequilibrium

textures are sieve-textured plagioclase, reverse zoning in orthopyroxene, breakdown of amphibole and clinopyroxene-rimmed quartz (*e.g.* Singer *et al.* 1995; Tepley *et al.* 1999; Nakagawa *et al.* 2002; Browne *et al.* 2006b). Disequilibrium may be caused by variable heating of the host magma from input of hotter magma (*e.g.* Tepley *et al.* 1999), or incorporation of the host phenocrysts into the incoming magma (*e.g.* Ruprecht & Wörner 2007), which may then be recycled back into the host magma via disaggregation (*e.g.* Clynne 1989, 1999; Browne *et al.* 2006b; Humphreys *et al.* 2009). Combined textural, petrological and geochemical analysis of magmatic enclaves and coexisting phenocrysts can therefore provide insights into the nature of the mixing magmas, the dynamics of the mingling process, and changes that may be occurring during mixing.

Soufrière Hills represents a unique opportunity to study the process of magma mingling in an active system. Magma intrusion at depth appears to have been quasi-continuous throughout the eruption, based on excess sulphur emissions (Edmonds *et al.* 2001, 2010) and inflation during eruptive pauses (Mattioli & Herd, 2003; Elsworth *et al.* 2008). A recent increase in the abundance of mafic enclaves may hint at changes in the magma mingling dynamics in Phase III (Barclay *et al*. 2010). Phases IV (July 2008 – Jan 2009) and V (Oct 2009 - Feb 2010) marked a change at SHV: eruptive phase length reduced from years to months and the average extrusion rate increased (Wadge *et al*. this volume). We present geochemical, textural and petrological analyses of mafic enclaves from Phase IV and V, alongside results from fieldwork. This work provides a window into syn-eruptive magma mingling processes.

Geological Background

Soufrière Hills Volcano (SHV) is located on the island of Montserrat in the Lesser Antilles island arc. The current eruption at SHV has been ongoing since July 1995 with five phases of andesitic dome-forming lava extrusion to date (Wadge *et al*. this volume). SHV andesite is porphyritic (30-40%) and is described in detail in prior studies (Devine *et al*. 1998; Barclay *et al*. 1998; Murphy *et al*, 2000; Couch *et al*. 2000; Humphreys *et al*. 2009). The phenocryst assemblage is plagioclase + hornblende + orthopyroxene + Fe-Ti oxides and minor quartz and rare zircon crystals, whereas the groundmass assemblage is plagioclase + orthopyroxene + clinopyroxene + Fe-Ti oxides, and interstitial glass is rhyolitic in composition. The andesite temperature, as bracketed by quartz and amphibole stability is ~830-870 ^{o}C (Barclay *et al*.

1998). Within the andesite at SHV mafic enclaves have been ubiquitous (Murphy *et al*. 1998, 2000; Harford *et al.* 2002; Barclay *et al*. 2010). Geochemically, SHV andesite compositions have been modelled as the result of fractional crystallisation of equal proportions of amphibole and plagioclase from the South Soufrière Hills basalt (erupted in the south of the island, ~130Ka; Zellmer *et al.* 2003; Harford *et al.* 2002). The SHV mafic enclaves and the South Soufrière Hills basalt are geochemically distinct with different REE trends and are not related by crystallisation (Zellmer *et al.* 2003).

The presence of mafic enclaves in SHV andesite is ascribed to the interaction between mafic magma and the andesitic host magma, which is perhaps the trigger and driver for the current eruption (Devine *et al.* 1998; Murphy *et al.* 1998; Murphy *et al.* 2000; Couch *et al.* 2001). It has been proposed that the initial intrusion of mafic magma underplated the andesitic magma (Murphy *et al*. 2000). A strong viscosity contrast exists between the highly crystalline andesite magma and phenocryst-poor mafic magma, so mechanical mixing is likely to be inhibited significantly (Sparks *et al.* 2000). Enclaves may have formed when fragmented dykes and blobs of less dense mafic material were injected into the overlying andesite (Murphy *et al.* 2000). The remobilisation of the andesitic magma may have taken place via initial conduction of heat across the mafic-andesite boundary followed by the development of instabilities and convection in the andesitic magma (Couch *et al.* 2001). An alternative model suggests that the remobilisation of the andesite (essentially a crystal mush) takes place by 'gas sparging', involving the upward migration of a hot fluid volatile phase derived from the mafic intrusion (Bachmann & Bergantz 2006). This fluid transports heat by advection, which is more efficient over shorter time-scales than conduction and may occur alongside limited mafic-silicic mingling, making this model consistent with observations of 'cryptic' mafic component of ~6% by volume in Phase III products (Humphreys *et al*. 2009; in press) and of excess gas (Edmonds *et al*. this volume).

Questions still remain concerning the dynamics of the mingling between the two magmas at SHV. Although different enclave types have been recognised in an earlier eruptive phase (Barclay *et al*. 2010), there has been little attempt to decipher the differing petrological and textural features between types. Prior work on enclave petrology has focussed predominantly on Phases I to III. Eruptive phase length has altered in Phases IV and V (Wadge *et al*. this volume), and therefore an additional aim of the work is to evaluate any changes in enclave petrology relative to the early stages of the eruption that might allow us to infer changes in magma reservoir conditions.

Methods

Samples of andesite and mafic enclaves were collected from a wide range of locations around SHV from deposits emplaced during Phase V activity (Table 1). Samples collected from the February 11th 2010 dome collapse deposits in the Trant's area are likely to have originated from a combination of Phase III, IV and V domes. Although minor Phase III deposits were incorporated into the collapse (Stinton *et al*. this volume), the distinctive Phase III lava described by Barclay *et al.* (2010) is inferred only to be a minor component of the flow deposits based on field observations. The significantly larger extruded volume in Phase V ($\sim 74 \times 10^6$ m^3; Stinton *et al*. this volume) compared to Phase IV ($\sim 39 \times 10^6$ m^3; Wadge *et al*. this volume), implies that many of the samples collected from the February 11th dome collapse were derived from Phase V. Samples that were collected from pyroclastic flow deposits in Aymers and White River are derived from Phase V (Stinton *et al*. this volume). Pumice was sampled from across Phase V activity (Oct 2009 – Feb 2010). Phase IV samples are from the January 3rd 2009 vulcanian explosion (Table 1).

Estimation of macroscopic enclave volume fraction

Enclave abundance was estimated using both macroscopic point counting and image analysis in the Phase V deposits. Nine lava blocks from the February 11th 2010 dome collapse deposits in the Trant's and Streatham areas (see map: Wadge *et al.* this volume) were analysed using both methods. Selection of the blocks was random, apart from requiring a relatively exposed and flat surface for analysis. Furthermore, to assess potential anisotropy in enclave fabric or abundance, two faces of a single block were analysed. For macroscopic point counting a grid of 1 m^2 with 2 cm intervals on each axis (Fig. 1b) permitted us to count up to a total of 2601 points per site. Spacing interval was chosen on the basis of the average size of enclaves, most are <10 cm in diameter (Fig. 2). The minimum size of enclaves counted was 1 cm (smaller enclaves could not be distinguished from crystal clots/glomerocrysts in the field). In addition to enclave abundance the size and shape of enclaves were also measured. Using photographs of the same 1 m^2 area, enclaves were isolated digitally from the andesite using ImageJ software. The isolated area fraction occupied by the enclaves was then calculated and compared to the point counting results. Image analysis yielded similar percentages, but consistently a little lower in comparison to the point counting method (by a mean of 1%). The slight underestimation of the image

analysis method is due to our inability to resolve the small enclaves (<2 cm) in the images, but is within standard error. We refer to the values obtained by the point counting method for enclave abundances.

Laboratory Analytical Methods

Seventy-four mafic enclaves and andesite samples from Phases IV and V were crushed and powdered for X-Ray Fluorescence (XRF) analysis to determine major and trace element concentrations at the University of East Anglia using a Bruker AXS S4 Pioneer. Standard deviations are <1% for all major oxides, apart from MgO and P_2O_5, which are <2%. Trace element accuracy is <2%, apart from Sc and Ce at <7% and <4% respectively. The diameters of enclaves analysed ranged from 3.3- 23.8 cm (Table 1). We also analysed different splits of the same samples, to rule out artefacts resulting from the relatively small sample size. Standard deviations are <1% for SiO_2, Al_2O_3, P_2O_5, Na_2O and Sr, all other major and trace element oxides are <5%. However, a single run of sample MT27 did produce anomalously high standard deviation values for K_2O and Ba of 15% and 31% respectively. The minimal deviations seen between different splits of the same sample were not great enough to explain the range of compositions as also concluded by Zellmer *et al.* (2003).

Thin sections of 40 samples were cut from dome rock and pumice. In enclave sections andesite-enclave margins were included, as well as the interior of large enclaves (>10 cm) to examine heterogeneity across enclaves. Secondary Electron Microscope (SEM) images were collected using Jeol JSM-5900LV at University of East Anglia, operating at an accelerating voltage of 20 kV and a working distance of 10 mm. Electron probe analysis was undertaken at University of Cambridge using a Cameca 5-spectrometer SX-100 instrument. Major elements of minerals were analysed using a 15 kV, 10 nA focused beam, and trace elements using a 15 kV, 10 nA beam. Standard deviations are <0.6% for all major and trace elements. Glasses were analysed using a 10 μm spot size with a 15 kV, 2 nA and 10 nA beam for major and trace elements respectively. Standard deviations are <0.9% for SiO_2 and Al_2O_3, and <0.4% for all other major and trace elements.

We measured plagioclase phenocryst size, type, and rim and sieve-texture thickness by analysing representative different enclave types. We used a total of six thin sections, one type A and the rest type B. We examined a wider range of Type B samples due to a greater

191 degree of heterogeneity across this enclave type. However, we also checked the results
192 against other type A samples to ensure that there was no bias towards the sample analysed**.**
193 We ruled out the possibility of a 2D sectioning of 3D crystals artefact as the overriding cause
194 of differing rim widths, as we observe a positive correlation between rim width and the
195 proportion of sieved inherited phenocrysts in different enclaves (see Fig. 3).

196 **Results**

197 The andesite erupted in Phase V of the eruption is porphyritic with a fine-grained
198 groundmass, and contains mafic enclaves as in earlier phases (Fig. 1) (Murphy *et al*. 1998,
199 2000; Harford *et al.* 2002; Barclay *et al*. 2010). Some andesite blocks contain distinctive
200 streaked highly crystalline layers of amphibole and plagioclase. Pumice is porphyritic with a
201 fine-grained groundmass and often contains mafic enclaves.

202 Total measured mafic enclave abundances within andesitic Phase V blocks range
203 from 2.9% to 8.2% from point counting, with a mean of 5.6% (Table 2). The size of
204 individual enclaves ranges from 1 to 80 cm; however, ~95% of the enclaves were <10 cm in
205 apparent diameter (Fig. 2). We categorised Phase V enclaves into three broad types that were
206 readily identifiable in the field using characteristics such as phenocryst proportions, the
207 nature of the margin between enclave and andesite, vesicularity, enclave size and shape, and
208 groundmass size and colour (Table 3). The classification scheme applied by Barclay *et al.*
209 (2010) is insufficient to describe the large textural diversity of the Phase V enclaves.

210 Type A enclaves are characterised as phenocryst-poor, vesicle-rich, with dark grey
211 groundmass and chilled margin (Table 3, Fig. 1). In the field these enclaves are readily
212 identified by their dark grey colour caused by the fine-grained groundmass composition.
213 Type A enclaves are typically ellipsoidal to sub-angular in shape, with occasional fingers of
214 the enclave material protruding into the andesite. Commonly the smaller (1-5 cm) angular
215 enclaves without evident chilled margins are clustered, suggesting that they are fragments of
216 a larger enclave that disaggregated mechanically after formation. Type A enclave volume
217 fraction reaches 46 % (with a mean of 22 %) of the total number of enclaves measured (Table
218 2). These have the smallest mean diameter of all the enclave types measured (2.3 cm),
219 although large enclaves over 18 cm were also measured (Fig. 2).

220 Type B enclaves are characterised as phenocryst-rich, vesicle-poor, with a light grey
221 groundmass and indistinct margins (Table 3, Fig. 1). In the field, type B enclaves are a lighter

grey than type A, and resemble most closely the host andesite in colour and texture (Fig. 1). They are generally ellipsoidal and well-rounded, although a few (<5 %) are angular in shape. Type B enclaves dominate across most of the analysed blocks, and represented 31% to 100% (with a mean of 64%) of the total enclaves measured. Their size distribution is strongly positively skewed from the norm with most <6 cm, (with a mean of 3.4 cm; Fig. 2).

Type C enclaves are composite and are characterised by distinct textural zones akin to types A and B (Table 3). Type C enclaves were present in all blocks examined except for block 5, with variable abundances of 0-41% (mean; 14%; Table 2). The size distribution of type C enclaves shows a weaker positive skew from the norm towards smaller sizes, (with a mean of 4.4 cm; Fig. 2). Below 2 cm composite textures were difficult to identify, which may be a factor in the increased mean size in comparison to other enclave types.

Distribution of enclaves is not even through the blocks; enclaves tend to cluster together, particularly in the smaller size fractions. Heterogeneity is observed both between blocks and within a single block; *e.g.* for block 1a-b, where two faces of the same block were measured, block 1a had a lower abundance of enclaves (3.5%), relative to the other face, block 1b (6.1%, Table 2). Furthermore, type A was absent from block 1a, but type A enclaves constituted 30% of the total in block 1b (Table 4), and of those, 66% were <2 cm (Fig. 2). This suggests localised clustering both of enclaves and enclave types.

Petrological and Textural Analysis

Following the criteria set out in Murphy *et al*. (2000), the term phenocrysts is used for crystals with major axis >300 μm, microphenocrysts 100-300 μm, and microlites <100 μm for the andesite and enclaves. The compositions of minerals from Phase V andesite are similar to those from earlier eruptive phases and there is no major change in andesite assemblage (Murphy *et al*. 2000; Humphreys *et al.* 2009). Mafic enclaves have a diktytaxitic groundmass framework of elongate, randomly-oriented crystals (Fig. 1d). This groundmass consists of plagioclase ± clinopyroxene ± high-Al-amphibole ± orthopyroxene. Fe-Ti oxides are observed throughout, and are often more abundant near inclusion margins. Titanomagnetite is the most common oxide, but ilmenite is also present. Trace amounts of apatite are often observed as inclusions in titanomagnetite and plagioclase-inherited phenocrysts (see below). Variable amounts of interstitial rhyolitic glass (71-78 wt% SiO_2) are found within the enclaves. Clinopyroxene (Mg# ~75) occurs as either the breakdown product

of amphibole, or as reaction rims on inherited orthopyroxene phenocrysts, or in the groundmass of the inclusions. The degree to which the framework is interlocked is usually correlated negatively with the amount of glass, disruption of vesicles and sizes of the groundmass crystals.

Large crystals (~2-3 cm) of plagioclase, amphibole and orthopyroxene are present in the mafic enclaves (Fig. 1d); most exhibit textural and compositional evidence that they have been inherited from the andesite (Murphy *et al.* 2000; Humphreys *et al.* 2009). We refer to these as inherited phenocrysts as they are not antecrystic or xenocrystic in origin. Following Murphy *et al.* (2000), the large inherited plagioclase phenocrysts in the enclaves can be split into two main types. Type 1 comprise large oscillatory zoned sodic phenocrysts (An_{49-57}) with calcic rims (An_{69-80}) 40-47 μm thick, similar to the type 1 and 2 plagioclases in the andesite (after Murphy *et al*. 2000). Type 2 are reverse-zoned dusty sieve-textured phenocrysts, where the sieve-texture (of thickness 70 μm to extending to the crystal core) is overgrown by a clear calcic rim (of thickness 0-230 μm) and comprises glass and high-anorthite (An_{70-90}) plagioclase. Smaller crystals (<1000 μm) have a pervasive sieve-texture. Rim width is typically largest where the degree of sieve texture is highest (Fig. 3). Low anorthite compositions (An_{49-57}) of the cores in both plagioclase types are identical to andesite phenocrysts compositions observed throughout the eruptive phases (Murphy *et al.* 2000; Humphreys *et al.* 2009). Core-to-rim transects across inherited plagioclase phenocrysts show a sharp increase in X_{An}, FeO and MgO at the rim. Inherited amphibole phenocrysts are Mg-hornblende (Leake *et al.* 1997), identical to low Al_2O_3 (6-8 wt %) amphiboles phenocrysts in the andesite. They are often variably opaticised, or partially reacted, with plagioclase and clinopyroxene overgrowths, indicating instability due to heating, rapid decompression or shallow storage in the dome (Garcia & Jacobson 1979; Murphy *et al.* 2000; Rutherford & Devine 2003; Browne & Gardner 2006; Buckley 2006; Plechov *et al*. 2008). Inherited orthopyroxene phenocrysts commonly have clinopyroxene overgrowths, Fe-Ti oxide inclusions, are typically reverse-zoned, with Mg# 58-74 identical to the andesite orthopyroxene compositions (Murphy *et al.* 2000; Humphreys *et al.* 2009). Rare embayed quartz phenocrysts with rims of clinopyroxene were also observed. Rare zircon crystals are also present in some enclaves.

Type A Enclaves

In thin section, type A enclaves (Table 3 and Fig. 4) are defined by a fine-grained groundmass, high vesicularity (19-40%, Fig. 5), chilled margins and low abundance of inherited phenocrysts (0 – 8.6%, Table 4, Fig. 6). The framework consists predominantly of plagioclase, with acicular amphibole and clinopyroxene also present. In the framework plagioclase disequilibrium features similar to a sieve texture can be seen developing in the cores of many microphenocrysts. These are enclosed by rims of clear plagioclase of composition An_{77-89} (Table 5, Fig. 4d). The framework amphibole (~13-15 wt % Al_2O_3, Table 5) is magnesio-hastingsite to pargasite (Leake *et al.* 1997), and typically has reaction rims of clinopyroxene that range from 5 μm thick to sometimes pervading the entire crystal (Fig. 4e). In Phase I the presence of framework amphibole was interpreted to correspond with larger enclave sizes (Murphy *et al.* 2000); this appears not to be the case in Phase V. Framework amphibole is present irrespective of the size of the enclave. Glass abundance is low (<5%), but is concentrated near vesicles and chilled margins. It contains on average 75wt % SiO_2 and 3.8 wt % K_2O (Table 5 and Fig. 7). Chilled margins are typically present, defined by a decrease in groundmass grain size towards the boundary, which is sharp to weakly gradational. Across large enclaves, inherited phenocryst abundances can be spatially extremely variable with densely clustered plagioclase phenocrysts associated with regions of increased enclave vesicularity. Type 1 plagioclase (with minor disequilibrium textures) is usually absent with predominantly type 2 (sieve-textured) dominating (Table 4). The rims on type 2 crystals range from 132–230 μm thick, which are the thickest rims measured in all the enclave types (Fig. 3). The rims of the inherited phenocrysts have high anorthite contents, of An_{80}-An_{90} (Table 5). Inherited amphibole phenocrysts are commonly completely opaticised with very little amphibole remaining, or have been almost completely replaced by clinopyroxene and plagioclase reaction products. Inherited phenocrysts are rarely observed transecting the boundary in this enclave type.

Type B Enclaves

Type B enclaves (Table 3 and Fig. 8) are defined by a variably sized fine to medium-grained groundmass, low to medium vesicularity (9-19%, Fig. 5), diffuse margins, and medium to high inherited phenocryst abundance (16.5-26%, Fig. 6 and Table 4). As with all enclave types the framework is predominantly plagioclase (An_{65-75}), which have lower X_{An} values in comparison with type A framework-phase plagioclase (An_{77-89}). High-Al framework

amphibole is typically absent, but occasionally present in enclaves with lower abundances of inherited phenocrysts (*i.e.* those that are closest to the type A enclaves). Glass is rare (<5%), and contains on average 77 wt% SiO_2 and 2.9 wt% K_2O (Table 5; Fig. 7), and is typically pooled near large vesicles where present. Orthopyroxene microlites (Wo_{2-4}, Fs_{38-40}, En_{56-60},) and calcic plagioclase microlites are sometimes observed growing outwards from vesicle walls (Fig. 8c). Some enclaves have large elongated vesicles, (~4 cm) with some vesicles disrupting the diktytaxitic framework, where crystals close to larger vesicles appear to have been bent after formation. Crystals (microlites or inherited phenocrysts) are regularly seen transecting enclave margins (Fig. 8). Type 2 inherited plagioclase phenocrysts dominate (Table 4); overall rim thickness (27-113 μm) is smaller in comparison to type A enclaves (see above) and is variable between different enclaves (Fig. 3). Inherited amphibole phenocrysts have variable disequilibrium textures: phenocrysts are either completely opaticised, broken down to clinopyroxene and plagioclase, or have undergone only minor disequilibrium. Rare inherited quartz with clinopyroxene overgrowth rims are also observed.

Type C Enclaves

Type C enclaves are composite, with at least two distinct different textural zones with respect to colour, vesicularity, and inherited phenocryst assemblage. Sample MT08 for example has a dark grey interior surrounded by a lighter grey exterior (Fig. 8e-f). The dark grey interior is somewhat similar to the type A enclaves, with a diktytaxitic groundmass framework composed of plagioclase (~An_{84}, Table 5), amphibole (~14 wt % Al_2O_3, Table 5) and clinopyroxene, and a mean vesicularity of 23.9%. Inherited phenocryst abundance is low (12.6%); type 2 inherited plagioclase phenocrysts are dominant. The lighter grey outer portion resembles type B enclaves, with a diktytaxitic framework of plagioclase (~An_{72}) and clinopyroxene; this portion does not display the same degree of crystal interlocking as the darker interior portion. Sparse high-Al amphibole laths are also observed in the outer portion close to the margin with the interior portion, typically where the margin is more diffuse. Furthermore, at the most diffuse margins plagioclase microphenocrysts are often observed. Vesicularity is lower in the outer portion relative to the interior portion (17.2%). Inherited phenocryst abundances are high (26.5%), dominated by plagioclase type 2, but type 1 is also present. Inherited amphibole and orthopyroxene are also present, which typically display more subtle disequilibrium textures than in the interior portion. The glass fraction is between

5 and 10%, and it is higher in the interior portion. Glass composition is similar to the type B enclaves in both portions, although the interior portion has slightly lower mean (74 wt% SiO_2) to the exterior (75 wt% SiO_2; Table 5, Fig. 7). The margin between the exterior portion and the host andesite is diffuse, with phenocrysts transecting the margin.

Enclaves In Pumice

Enclaves in pumice are extremely vesicular compared to those in lava dome blocks. The margins of the enclaves are lined with large coalesced vesicles, inhibiting identification of the original (pre-decompression) margin texture. Large amphiboles in the enclaves sometimes display boudinage textures similar to those seen in the andesite pumice (Giachetti *et al.* 2010). We do not include enclaves in pumice in our classification scheme owing to the large degree of textural overprinting of features by late-stage ascent processes.

Geochemistry

We present whole rock major and trace element geochemical data for the mafic enclave types discussed above and andesite from Phases III, IV and V, and examine geochemical differences between the enclave types, as defined on the basis of their texture and petrology.

We first compare phases IV and V major and trace element composition with the earlier phases of the eruption. Phases IV and V mafic enclaves and host andesite continue to fall on the linear array of most major elements, as established in previous phases (Fig. 9) (Murphy *et al.* 2000; Zellmer *et al.* 2003). Although phase V andesite SiO_2 is slightly lower on average than earlier phases, values still lie within the range of data from the previous phases (Fig. 9). However, the compositional gap in SiO_2 between the mafic enclaves and the andesite observed in phases I-III, no longer exists in phase V (Fig. 9). Phase V andesite and mafic enclaves do not continue the trend of increasing MgO and decreasing Fe_2O_3 established between Phases I to III (Barclay *et al*. 2010) (Fig. 9), but instead remain similar in composition to Phase III.

The different categories of enclaves, as defined by their textural and petrological features, are also distinct in terms of bulk geochemistry. Although the type A and B enclaves fall on a single linear array with the andesite with no compositional gaps, each type plots in a distinctive field for all major elements (Fig. 10). Type A enclaves occupy a narrow compositional range (49.7-52.4 wt % SiO_2), whereas type B enclaves have a much broader range (53-58 wt% SiO_2) (Fig. 10). Trace element distributions in the enclaves studied are

consistent with previous studies. For example, Zr is positively correlated with SiO_2, whilst V is negatively correlated (Fig. 10).Type A enclaves have systematically higher compatible trace element contents, and lower incompatible trace element contents, than the type B enclaves (Fig. 10).

In the composite Type C enclaves, interior portions are less evolved (52.7 to 55.4 wt% SiO_2) and the outer portions are more silicic (55.8 to 58.1 wt % SiO_2), with one point lying in the host andesite field. The relative difference between the two portions is typically about 3 wt %, irrespective of absolute SiO_2 values. However, Type C enclave bulk compositions plot entirely within the field for Type B enclave points (Fig. 10).

Glass compositions are rhyolitic (71-79 wt % SiO_2, Table 5) for the mafic enclaves similar to prior eruptive phases and lie within established trends (Humphreys *et al.* 2010; Murphy *et al.* 2000). There are some notable differences between the enclave types of Phase V. Type A enclaves have a wide scatter of K_2O compositions in comparison to types B and C, but is higher on average (Fig. 7a). Type A enclaves also have on average higher FeO and MgO (Fig. 7b). In contrast type B enclaves have low FeO and MgO compositions. Type C inner and outer enclave portions glass compositions were measured. In most elements measured there is an observed difference between the two portions. The inner portion compositions plot within the type A field in FeO, MgO and TiO_2, whereas the outer portion compositions tend to plot within the type B field in K_2O (Fig. 7a). There are however considerable overlap between the fields in FeO and MgO (Fig. 7b).

Summary

In summary we find that there are distinctive textural, petrological and geochemical differences between the phase V enclave types (Table 3). Type A enclaves are least evolved with a narrow compositional range, a low inherited phenocryst fraction, high vesicularity and with chilled margins. Type B enclaves have a broader, but more silicic compositional range, a high inherited phenocryst fraction and no chilled margins. The composite Type C enclaves have a more mafic inner portion with an affinity to type A, and an outer more silicic portion akin to Type B. We examine the constraints on the formation of the differing enclave types to help constrain a model of the mingling dynamics between the andesitic and mafic magmas in Phase V.

Discussion

In general, the low crystallinity and inherited phenocryst content, chilled margins, and relatively restricted primitive geochemical composition suggests that the type A enclaves are close to an end-member mafic magma that quenched rapidly on contact with the andesite. In contrast, type B enclaves, with their much higher inherited phenocryst content, lack of chilled margins and more evolved compositions, are significantly hybridised. Type C enclaves are composite, with a more mafic interior indicating dynamic mingling between types A and B. Below we discuss in detail the constraints on the formation of these three enclave types and implications for the nature of magma mixing at Soufrière Hills Volcano.

Geochemical constraints on end-member magma compositions

Work by Zellmer *et al*. (2003) indicates that the mafic magma is formed by closed-system fractional crystallisation of amphibole (70%) and plagioclase (30%). The type A enclaves are the least evolved of the enclave types, with low incompatible trace element concentrations; we therefore interpret them to be closest to a hypothesised low SiO_2 mafic magma end-member. However, the presence of inherited phenocrysts indicates that even these least evolved enclaves are already hybridised.

The Type B enclaves are more evolved in comparison to type A, but reflect a broad range of compositions. The strongly linear compositional arrays in major elements (Al_2O_3, CaO *etc.*) and trace elements (Zr, Ba *etc.*) through the mafic enclaves to the host andesite in Phase V (Fig. 10), supports a mixing relationship between the mafic and andesite end-members. This suggests that type B enclaves reflect a continuum of degrees of mixing. Nonetheless, we also observe that there is bimodal distribution between the total inherited phenocryst fraction between types A and B. Using the average core compositions of inherited plagioclase and amphibole phenocrysts, we find that addition of the phenocrysts to the mafic melt should drive the melt to more mafic compositions (Fig. 10). However, the trend between Type A and B is towards more evolved compositions with increasing phenocryst abundance (Fig. 6), suggesting that the phenocryst incorporation has relatively little impact on bulk composition and that mixing is the dominant process.

The relatively homogeneous rhyolitic composition of glass in the mafic enclaves could indicate that felsic melt from the andesite has infiltrated into the mafic enclaves, or may

441 simply be the result of extensive crystallisation of a mafic melt. Engulfment of inherited
442 phenocrysts must also be accompanied by liquid assimilation from the andesite host, which
443 will affect the bulk composition of the mafic enclaves. If this is the case, type B melt
444 compositions may reflect a localised hybrid starting composition before framework
445 crystallisation in contrast to the type A melt. At Narugo Volcano, Japan compositional
446 similarity between glasses in the host magma and mafic inclusions is interpreted as evidence
447 of infiltration of the host magma melt into a boundary layer before enclave formation (Ban *et*
448 *al.* 2005). Although glass compositions of the andesite and enclaves are both rhyolitic and
449 overlap at SHV, there is a clear difference between the types A and B glass in K_2O (Fig. 7a).
450 Type B is somewhat similar to the andesite (Humphreys *et al*. 2010) and less variable than
451 type A glass. This may imply that the melt in Type B enclaves is more homogenised in
452 comparison to Type A allowing K_2O time to re-equilibrate with the andesite host (Humphreys
453 *et al.* 2010). The diffusive timescale of K has been calculated to be 32 days for rhyolitic
454 compositions across a length-scale of 1 cm (Humphreys *et al*. 2010). Therefore, preservation
455 of the higher K_2O glass composition of the type A enclaves may be attributed to a shorter
456 timescale of mixing than type B.

457

458 ***Petrological and textural mingling constraints***

459 The presence of chilled margins, lower inherited phenocryst abundance, higher plagioclase
460 anorthite compositions and ubiquitous presence of high Al-amphibole in the framework
461 crystals of type A enclaves relative to the type B enclaves all suggest that controls on the
462 formation differed between the enclave types.

463 Engulfment of phenocrysts from the host magma by an incoming magma has been
464 observed elsewhere *e.g.* Unzen, Kameni, Chaos Craggs (Clynne 1999; Browne *et al.* 2006a;
465 Martin *et al.* 2006a; Feeley *et al.* 2008). Previous work on inherited plagioclase phenocrysts
466 from SHV demonstrates a positive correlation between iron and anorthite content at the
467 phenocryst rim (Humphreys *et al.* 2009). The disequilibrium textures and rim growth on the
468 plagioclase was therefore probably caused by the incorporation of the inherited phenocrysts
469 into a high-calcium melt (Ruprecht & Wörner 2007; Humphreys *et al.* 2009) rather than by
470 decompression and degassing (Coombs *et al.* 2000). The presence of inherited phenocrysts in
471 the type A enclaves, where chilled margins would significantly inhibit mass exchange
472 between the enclave and andesite (Blake & Fink 2000), indicates that the majority of

phenocryst incorporation must have taken place before chilled margin formation. The higher inherited phenocryst fraction in the type B enclaves (16.5-26%) in comparison to the Type A enclaves (0 – 8.6%) indicates a greater interaction with the andesitic melt prior to enclave formation (Fig. 6). Differing rim and sieve-texture disequilibria widths of the inherited plagioclase phenocrysts in individual enclaves may reflect differing time-scales of engulfment or conditions of residence in the mafic melt (Fig. 3). In contrast, at Unzen, Japan, uniformity of calcic rim widths and sieve-textures of inherited plagioclase phenocrysts are interpreted as indication of a single episode of engulfment of phenocrysts into enclaves (Browne *et al.* 2006b).

The effect of adding inherited phenocrysts on the viscosity of the mafic magma was estimated using the Einstein-Roscoe relation for effective viscosity, with melt viscosity calculated using the empirical model of Giordano *et al*. (2008). We find that the addition of the inherited phenocrysts increases the effective viscosity of the mafic magma and dominates over the effect that the associated temperature reduction would have (Fig. 11). However, even with the maximum observed volume of 25 % inherited phenocryst fraction in the type B end-member a relative viscosity contrast between the andesite (45-55 vol% phenocrysts) still exists. Prior to mafic magma crystallisation, the viscosity will be lower than the andesite viscosity. However, after quench crystallisation, where crystal content can be >90% vol, enclave viscosity will be greater than andesite viscosity and this will inhibit mixing (Sparks & Marshall 1986). The inherited phenocryst content also contributes to a viscosity contrast between types A and B, which implies that mixing would be inhibited between the two types (Fig. 11).

The diktytaxitic framework observed in both type A and B enclaves demonstrate that quench crystallisation took place during thermal equilibration with the andesite. This implies that a temperature contrast must exist between the andesite and even the most hybridised mafic melt prior to enclave crystallisation. However, textural and petrological differences show that this contrast was variable during formation of types A and B enclaves. An overall higher anorthite content of type A enclave inherited plagioclase phenocryst rims, microphenocrysts and microlites in comparison to type B enclaves, could be indicative of crystallisation under hotter conditions or more H_2O-rich conditions. Differing sized enclaves and types may take different times to equilibrate thermally (Bacon 1986), and therefore phenocryst disequilibrium is likely to be slightly different between enclaves. However, inherited plagioclase phenocrysts' sieve-textures and rims in type A enclaves are consistently

506 thicker (Fig. 3). This hints at higher temperatures, rather than a longer residence time of the
507 inherited phenocrysts in comparison to type B enclaves, which may be consistent with
508 inferences from the residual glass composition. Furthermore, this process would be limited by
509 the rapid cooling that would take place as the enclave reached thermal equilibrium (Bacon
510 1986; Sparks & Marshall 1986). Chilled margins reflect rapid cooling caused by a significant
511 temperature contrast between the enclave and host magma, with the enclave largely liquid
512 during formation (Bacon 1986; Sparks & Marshall 1986; Clynne 1999). We therefore infer
513 that type A enclaves not only formed from a hotter melt than type B, but that formation was
514 the result of injection into the andesite as a liquid, where rapid cooling drove crystallisation
515 and formation of the chilled margins.

516 The lack of chilled margins in type B enclaves could result either from a smaller
517 temperature contrast between enclave and andesite, in comparison to type A, or from
518 mechanical abrasion of enclave margins caused by shear stress (Feeley & Dungan 1996). We
519 suggest that mechanical abrasion would be unlikely to remove all evidence of a chilled
520 margin. A reduced temperature contrast would prevent strong decrease in crystal size at the
521 chilled margin, and allows greater time for mass and chemical exchange during quenching
522 (Bacon 1986). A temperature contrast of 15-50 °C has been experimentally constrained to
523 produce similar textures to the type B enclaves during crystallisation in a layer at the silicic-
524 mafic interface (Coombs *et al*. 2002). Furthermore, variability in textures in the type B
525 enclaves may be a function of crystallisation depth below a mafic-silicic interface, as slower
526 cooling will take place further away from the boundary (Coombs *et al*. 2002; Martin *et al*.
527 2006a). This may indicate that quench crystallisation of the type B enclaves took place
528 before incorporation into the andesite and subsequent disaggregation (*e.g.* Eichelberger
529 1980; Martin *et al.* 2006a).

530 The ubiquitous presence of the high-Al amphibole laths in the type A as opposed to
531 the type B enclaves might be a function of melt volatile content. In several plutonic centres
532 such as the Cadillac Mountain Granite and the Pleasant Bay Intrusion, a positive correlation
533 between more hybridised (higher SiO_2) enclaves, with the absence of hornblende and
534 presence of clinopyroxene has been observed (Wiebe 1993; Wiebe *et al.* 1997). The change
535 from a hydrous to anhydrous assemblage is attributed to the exchange of H_2O between stably
536 stratified mafic and silicic layers (Wiebe *et al.* 1997). Amphibole compositions in the type A
537 enclaves have 6.4-9.0 wt % H_2O calculated using the method of Ridolfi and Renzulli (2011).
538 This is consistent with RhyoliteMelts modelling of a saturated water-rich mafic magma (>8

wt % H_2O), which reproduces the observed porosity and fraction of melt remaining in the type A enclaves (Edmonds *et al*. this volume). The lower porosity and abundance of amphibole in the type B enclaves might suggest a lower melt volatile content in comparison to type A. The presence of some high-Al amphiboles laths in the least evolved type B enclaves implies that the H_2O content was sufficient to allow limited amphibole crystallisation. Variability in the volatile content of the mafic magma might be also account for differences in the anorthite content of the plagioclase microphenocrysts between enclave types. Higher H_2O melt content can lead to higher anorthite content as opposed to just higher temperatures, which is consistent with the type A enclaves (*e.g.* Couch *et al.* 2003b). Alternatively, the high-Al amphibole might have had more time in the type B enclaves to resorb, which also might explain their absence.

The plagioclase framework microphenocryst disequilibria observed in the type A enclaves (Fig. 4c) could be created by a number of processes; (1) strong undercooling where melt is trapped in the skeletal structure of the crystals as they grow rapidly (2) decompression-induced disequilibria (Nelson & Montana 1992) (3) degassing-induced disequilibria (Frey & Lange 2011). As there is already evidence to suggest higher rates of cooling in the type A enclaves, the large temperature contrast could conceivably be the controlling process. However, destabilisation of some framework pargasitic amphibole rims indicated by breakdown to clinopyroxene may indicate decompression-induced disequilibria or shallow storage residence in the dome (Rutherford & Devine 2003; Browne & Gardner 2006; Buckley 2006).

The large coalesced vesicles in some of the type B enclaves suggest vesicle expansion caused by decompression or by longer timescales. Coalesced vesicles have been cited as evidence of overturn and subsequent breakup of a foam layer at the mafic-silicic interface (Martin *et al*. 2006a). Bent framework crystals also imply vesicle expansion after crystallisation (Martin *et al*. 2006a). This disruption to the enclave framework implies that the type B enclaves are perhaps disaggregated fragments of larger pieces (Martin *et al*. 2006a; Edmonds *et al*. this volume). This is further supported by the presence of clusters of small angular to sub-angular enclaves within andesite. In a sample of andesite from Phase III, Humphreys *et al.* (in press) calculated that the total cryptic abundance of material derived from disaggregation of mafic enclaves is approximately 6-7%, implying that this process is prevalent at SHV. Microlites or microphenocrysts of high-Al amphibole are very rarely

observed within the andesite, which lends support to the idea that it is largely or even exclusively this hybridised layer that is experiencing this level of disaggregation.

Type C Enclaves

Composite or mixed enclaves have been observed in previous eruptive phases (Barclay *et al.* 2010) as well as Phases IV and V. Composite enclaves are suggestive of more complex hybridisation mechanisms. The inner portion of the enclave used for this study has retained a compositional and textural identity similar to the more mafic type A. While the surrounding more silicic portion is texturally and compositionally similar to type B enclaves. The concentration of glass near the interior margin of the inner part of the enclave, together with the diktytaxitic framework present, suggests that hotter, more mafic magma is mingled into the cooler more silicic magma, whilst both are still fluid (Snyder *et al.* 1997). The presence of a few high-Al amphibole laths in the more silicic portion near the inner margin demonstrates that there has been limited mechanical exchange of melt and groundmass material between the two portions of the enclave. The enclave-andesite margin, with fingers of andesitic material intruding into the enclave indicates weak cooling of the silicic portion in contact with the host andesite. Composite enclaves may form as mafic magma 'pillows', surrounded by a thin film of hybrid material separating the mafic from the silicic magma (Blake & Ivey 1986; Snyder *et al.* 1997). The inner mafic portion will crystallise first, and then the surrounding hybridised portion preserving the interior mafic portion (Collins, 2000).

Phase V mingling model

We propose that the textural and petrological variations of the type A and B enclaves are created by differing formation mechanisms, partly influenced by the degree of mingling between the host andesite and intruding mafic magma, which in turn controls temperature and viscosity contrasts. In addition, the nature and timing of incorporation of the enclaves into the andesite may also play a role in the differences between the enclaves. In our model for enclave formation (Fig. 12), volatile-saturated mafic magma is injected into the chamber as a plume, and mixes with the host andesite to varying degrees, engulfing the andesite-derived phenocrysts and creating a hybrid mafic magma with a broad range of compositions. Type A enclaves formed at high rates of cooling and therefore may have formed at the plume margin (Browne *et al*. 2006a). The high viscosity contrast between the mafic and andesitic magma

602 end-members would prevent effective mixing (Fig. 11), but viscous shearing of the plume
603 margin could have taken place. Alternatively, blobs of less dense mafic magma might have
604 detached from the plume during injection into the andesite as a 'spray' quenching upon
605 incorporation into the andesite. Ponding of the intruding magma from plume collapse is likely
606 to have occurred either as a result of a decrease in the rate of injection (*e.g.* Eichelberger
607 1980; Sparks & Marshall 1986) or in the density contrast with the andesite (Feeley *et al*.
608 2008). This leads to the formation of a mafic hybrid layer where at the mafic-silicic interface
609 crystallisation-induced vesiculation occurred (Eichelberger 1980), from which type B
610 enclaves are derived (Fig. 12b). For enclave flotation to occur, the H_2O content of the
611 enclaves must be >6 wt % (Edmonds *et al*. this volume). Disruption of the mafic-silicic
612 interface may be result of (1) crystallisation-induced vesiculation, where the density of the
613 hybrid mafic magma reduced beneath that of the andesite and enabled overturn or (2) an
614 instability or plume of the mafic magma intruded through the hybrid layers destabilising and
615 inducing breakup, reproducing the cycle.

616 Composite enclaves may form from small plumes of vesicular, less dense, hotter
617 mafic material which could buoyantly rise and mingle within the overlying cooler hybridised
618 layers (Cardoso & Woods, 1999). The compositional and viscosity gap between types A and
619 B end-members would limit mixing (Fig. 11) and perhaps allow the composite enclaves to
620 form. These could form undercooled mafic pillows within the hybrid layer, which is then
621 intruded into the overlying andesite (Fig. 12c). However, this does not explain adequately the
622 presence of the inherited phenocrysts in the interior more mafic portion of the enclaves.

623 It is unclear if the timing of the processes forming the type A, B and C enclaves are
624 similar. The presence of the composite enclaves could imply multiple injections of mafic
625 magma, and suggest a temporal separation between types A and B. Differences in glass
626 compositions (Fig. 7), also may indicate longer mingling time-scales for the type B enclaves
627 in comparison to type A. In addition, differing degrees of inherited phenocryst disequilibria
628 within single enclaves might suggest temporal variations of the engulfment of phenocrysts
629 rather than a single intrusion. However, as SHV is a long-lived system with multiple
630 extrusive phases with evidence for quasi-continuous intrusion at depth, it is likely to
631 demonstrate dynamic mingling. We also cannot rule out that the differing enclave types may
632 be due to turbulent mingling processes rather than suggesting temporal differences.

633 Finally, we also cannot rule out the possibility that Type A and B enclaves may represent two
634 separate magmas rather than simply differences in the degree of hybridisation. This is
635 suggested by the clear differences in inherited phenocryst and vesicle abundances, glass
636 compositions, and melt volatile contents, although the linear major- and trace-element
637 compositional arrays do suggest variable hybridisation. The composite enclaves clearly
638 demonstrate that two-stage mixing has occurred. We might expect to see clear differences in
639 rare earth elements between the types, if these represent two separate magmas.

640

641 ***Comparison with earlier extrusive phases***

642 Observed changes in the eruptive phase length, mafic enclave abundances and bulk
643 geochemistry lead us to question whether there has been any temporal change in the nature of
644 the intruding or erupted magma in phases IV and V. The increased average SiO_2 bulk rock
645 composition of the mafic enclaves since phase III (Fig. 9), together with the dramatic increase
646 in compositional range of the enclaves (from basaltic to andesitic) (Fig. 9) means that there is
647 no longer a compositional gap between the mafic enclaves and host andesite. This suggests
648 that there has been an overall increase in the degree of hybridisation between the mafic and
649 andesitic magmas in Phases IV and V. Increased hybridisation of the mafic magma could be
650 related to lower degrees of cooling against the host andesitic magma, perhaps due to
651 successive replenishments of hotter mafic magma or continued transfer of heat from the
652 existing mafic source (Wiebe 1993; Wiebe *et al.* 1997; Collins *et al.* 2006; Turnbull *et al.*
653 2010). The effective viscosity contrast would also be reduced between the two magmas and
654 thus promote greater mixing between the two magmas, resulting in more hybridised enclaves
655 as the current eruption continues (Sparks and Marshall, 1986). If this explanation is correct,
656 continued heating must be relatively localised; otherwise we would anticipate observing
657 changes to the phenocryst rim compositions in the andesite in phase V, which we do not. We
658 also expect changes to the crystal size distributions of the mafic enclaves over time, although
659 this is beyond the scope of the current study.

660

661 **Conclusions**

662 We provide a complete petrological, textural and geochemical description of three distinct
663 mafic enclave populations in the Soufrière Hills andesite, from the eruptive products of

664 phases IV and V of the current eruption. Type A are basaltic with a narrow range of
665 compositions, and are recognised by the presence of chilled margins and high-Al amphiboles,
666 high vesicularity and high inherited phenocryst abundance. Type B have a broad range of
667 compositions (basaltic andesite), and are identified by a lack of chilled margins, low
668 vesicularity and high inherited phenocryst abundance, and rare to absent high-Al amphiboles.
669 Type C are composite with a more mafic interior zone, which is similar to the described type
670 A, and an exterior zone akin to type B. Analysis of bulk compositions, textures, enclave
671 petrology and viscosity demonstrates that differences between the enclave types are partially
672 the result of the degree of mingling between the andesite and mafic magmas. This in turn has
673 led to differing contrasts in temperature, viscosity, density and composition between the
674 enclave types. We interpret Type A to be close to a mafic end-member magma, while Type B
675 is significantly hybridised; Type C represents an interface between the two types.

676 We observe linear compositional arrays between Type A enclaves and the host
677 andesite; with type B enclaves reflecting a broad range of compositions on these arrays (Fig.
678 9). In addition, the presence of inherited phenocrysts confirms that all enclaves are hybridised
679 to some degree. The higher inherited phenocryst abundances in type B indicate a greater
680 degree of interaction with the host andesite. All enclaves contain rhyolitic matrix glass due to
681 crystallisation, but there are observable differences in composition between enclave types.
682 Variations in K_2O may reflect differing time-scales for mingling and reequilibration between
683 the enclave types.

684 The absence of the high-Al amphibole, and lower anorthite content of plagioclase
685 microphenocrysts in the Type B enclaves may be due to a lower melt volatile content in Type
686 B relative to Type A. The chilled margins in type A enclaves indicate that crystallisation and
687 formation was driven by rapid cooling with the andesite, while the more hybridised Type B
688 experienced slower cooling. Differences in degree of mingling probably arise from variations
689 in temperature, composition and viscosity contrasts between the andesite and mafic magmas.
690 Thus the distinct textural, petrological and geochemical differences between enclave types
691 reflect differing formation histories. The more mafic Type A enclaves were formed from an
692 injected plume of more primitive mafic magma, where limited mingling led to minor
693 incorporation of inherited phenocrysts. Continued mixing of the intruding mafic magma
694 resulted in a hybrid mafic magma, which ponded at the base of the chamber. The texturally
695 broad Type B enclaves represent differing fragments from within a disrupted hybrid layer
696 formed at the mafic-silicic interface. Composite enclaves represent two-stage mingling

between types A and B, where more mafic magma has intruded into the more hybrid magma layer reflecting temporal differences between them.

There is a suggestion that the degree of hybridisation has changed during the course of the current eruption, as reflected in the disappearance of the SiO_2 gap between the host and mafic enclaves bulk compositions in Phase V. This could be due to continued mafic replenishment causing localised reductions in the temperature contrast between the magmas as heat is transferred from the mafic intrusion to the andesite. This might permit localised increases in the degree of mixing between the mafic and andesite magmas.

Acknowledgements

MP acknowledges the support of a NERC studentship NE/H524506/1. MCSH acknowledges support from a Royal Society University Research Fellowship. We would like to thank all the staff at the Montserrat Volcano Observatory for their assistance during fieldwork. We also thank Bertrand Leze for analytical assistance. We thank Michael Clynne and Michel Pichavant for their constructive reviews, which helped to improve this manuscript.

References

BACHMANN, O. & BERGANTZ, G. W. 2006. Gas percolation in upper-crustal silicic crystal mushes as a mechanism for upward heat advection and rejuvenation of near-solidus magma bodies. *Journal of Volcanology and Geothermal Research* **149**, 85-102.

BACON, C. R. 1986. Magmatic Inclusions in Silicic and Intermediate Volcanic Rocks. *J. Geophys. Res.* **91**.

BAN, M., TAKAHASHI, K., HORIE, T. & TOYA, N. 2005. Petrogenesis of Mafic Inclusions in Rhyolitic Lavas from Narugo Volcano, Northeastern Japan. *Journal of Petrology* **46**, 1543-1563.

BARCLAY, J., RUTHERFORD, M.J., CARROLL, M.R., MURPHY, M.D., DEVINE, J.D., GARDNER, J. & SPARKS, R.S.J. 1998. Experimental phase equilibria constraints on pre-eruptive storage conditions of the Soufrière Hills magma. *Geophysical Research Letters* **25**, 3437-3440

BARCLAY, J., HERD, R. A., EDWARDS, B. R., CHRISTOPHER, T., KIDDLE, E. J., PLAIL, M. & DONOVAN, A. 2010. Caught in the act: Implications for the increasing abundanceof mafic enclaves during the recent eruptive episodes of the Soufrière Hills Volcano, Montserrat. *Geophys. Res. Lett.* **37**, L00E09. doi:10.1029/2010GL042509.

728 BLAKE, S. & FINK, J. H. 2000. On the deformation and freezing of enclaves during
729 magma mixing. *Journal of Volcanology and Geothermal Research* **95**, 1-8.
730 BLAKE, S. & IVEY, G. N. 1986. Magma-mixing and the dynamics of withdrawal from
731 stratified reservoirs. *Journal of Volcanology and Geothermal Research* **27**, 153-178.
732 BROWNE, B. L., EICHELBERGER, J. C., PATINO, L. C., VOGEL, T. A., DEHN, J., UTO, K.
733 & HOSHIZUMI, H. 2006a. Generation of Porphyritic and Equigranular Mafic Enclaves
734 During Magma Recharge Events at Unzen Volcano, Japan. *Journal of Petrology* **47**, 301-
735 328.
736 BROWNE, B. L., EICHELBERGER, J. C., PATINO, L. C., VOGEL, T. A., UTO, K. &
737 HOSHIZUMI, H. 2006b. Magma mingling as indicated by texture and Sr / Ba ratios of
738 plagioclase phenocrysts from Unzen volcano, SW Japan. *Journal of Volcanology and*
739 *Geothermal Research* **154**, 103-116.
740 BROWNE, B. L. & GARDNER, J. E. 2006. The influence of magma ascent path on the
741 texture, mineralogy, and formation of hornblende reaction rims. *Earth and Planetary*
742 *Science Letters* **246**, 161-176.
743 BUCKLEY, V. J. E., SPARKS, R. S. J. & WOOD, B. J. 2006. Hornblende dehydration
744 reactions during magma ascent at Soufrière Hills Volcano, Montserrat. *Contributions to*
745 *Mineral Petrology*. **151**, 121-140. DOI 10.1007/s00410-005-0060-5
746 CARDOSO, S. S. S. & WOODS, A. W. 1999. On convection in a volatile-saturated
747 magma. *Earth and Planetary Science Letters* **168**, 301-310.
748 CLYNNE, M. A. 1989. The disaggregation of quenched magmatic inclusions
749 contributes to chemical diversity in silicic lavas of Lassen Peak, California. Bull New
750 Mexico Bureau of Mines and Mineral resources, vol. **131**, p. 54
751 CLYNNE, M. A. 1999. A Complex Magma Mixing Origin for Rocks Erupted in 1915,
752 Lassen Peak, California. *J. Petrology* **40**, 105-132.
753 COLLINS, W. J., RICHARDS, S. R., HEALY, B. E. & ELLISON, P. I. 2000. Origin of
754 heterogeneous mafic enclaves by two-stage hybridisation in magma conduits (dykes)
755 below and in granitic magma chambers. *Geological Society of America Special Papers*
756 **350**, 27-45.
757 COLLINS, W. J., WIEBE, R. A., HEALY, B. & RICHARDS, S. W. 2006. Replenishment,
758 Crystal Accumulation and Floor Aggradation in the Megacrystic Kameruka Suite,
759 Australia. *Journal of Petrology* **47**, 2073-2104.

COOMBS, M. L., EICHELBERGER, J. C. & RUTHERFORD, M. J. 2000. Magma storage and mixing conditions for the 1953-1974 eruptions of Southwest Trident volcano, Katmai National Park, Alaska. *Contributions to Mineralogy and Petrology* **140**, 99-118.

COOMBS, M. L., EICHELBERGER, J. C. & RUTHERFORD, M. J. 2002. Experimental constraints on mafic enclave formation in volcanic rocks. *Journal of Volcanology and Geothermal Research* **119**, 125-144

COUCH, S., SPARKS, R. S. J. & CARROLL, M. R. 2001. Mineral disequilibrium in lavas explained by convective self-mixing in open magma chambers. *Nature* **411**, 1037-1039.

COUCH , S., HARFORD, C.L., SPARKS, R. S. J. & CARROLL, M. 2003b. Experimental constraints on the conditions of highly calcic plagioclase microlites at the Soufrière Hills Volcano, Montserrat. *Journal of Petrology* **44**, 1455-1475

DEVINE, J. D., MURPHY, M. D., RUTHERFORD, M. J., BARCLAY, J., SPARKS, R. S. J., CARROLL, M. R., YOUNG, S. R. & GARDNER, J. E. 1998. Petrologic Evidence for Pre-Eruptive Pressure-Temperature Conditions, and Recent Reheating, of Andesitic Magma Erupting at the Soufrière Hills Volcano, Montserrat, W.I. *Geophys. Res. Lett.* **25**.

EDMONDS, M., PYLE, D., OPPENHEIMER, C. 2001. A model for degassing at the Soufrière Hills Volcano, Montserrat, West Indies, based on geochemical evidence. *Earth and Planetary Science Letters* **186**, 159-173.

EDMONDS, M., AIUPPA, A., HUMPHREYS, M., MORETTI, R., GIUDICE, G., MARTIN, R. S., HERD, R. A. & CHRISTOPHER, T. 2010. Excess volatiles supplied by mingling of mafic magma at an andesite arc volcano. *Geochem. Geophys. Geosyst.* **11**, Q04005. doi:10.1029/2009GC002781.

EDMONDS, M., HUMPHREYS, M. C. S., HAURI, E., HERD, R., WADGE, G., RAWSON, H., LEDDEN, R., PLAIL, M., BARCLAY, J., AIUPPA, A., CHRISTOPHER, T., GIUDICE, G. & GUIDA, R. (this volume). Pre-eruptive vapour and its role in controlling eruption style and longevity at Soufrière Hills Volcano. *Geol Soc Memoir*.

EICHELBERGER, J. C. 1980. Vesiculation of mafic magma during replenishment of silicic magma reservoirs. *Nature* **288**, 446-450.

ELSWORTH, D., MATTIOLI, G., TARON, J., VOIGHT, B. & HERD, R. 2008. Implications of Magma Transfer Between Multiple Reservoirs on Eruption Cycling. *Science* **322**, 246-248.

FEELEY, T. C., WILSON, L. F. & UNDERWOOD, S. J. 2008. Distribution and compositions of magmatic inclusions in the Mount Helen dome, Lassen Volcanic Center, California: Insights into magma chamber processes. *Lithos* **106**, 173-189.

FREY, H. M. & LANGE, R. A. 2011. Phenocryst complexity in andesites and dacites from the Tequila volcanic field, Mexico: Resolving the effects of degassing vs. magma mixing. *Contributions to Mineralogy and Petrology* **162**, 415-445.

GARCIA, M. O. & JACOBSON, S. S. 1979. Crystal clots, amphibole fractionation and the evolution of calc-alkaline magmas. *Contributions to Mineralogy and Petrology* **69**, 319-327.

GIACHETTI, T., DRUITT, T. H., BURGISSER, A., ARBARET, L. & GALVEN, C. 2010. Bubble nucleation, growth and coalescence during the 1997 Vulcanian explosions of Soufrière Hills Volcano, Montserrat. *Journal of Volcanology and Geothermal Research* **193**, 215-231.

GIORDANO, D., RUSSELL, J.K. & DINGWELL, D.B. 2008 Viscosity of magmatic liquids: A model. *Earth and Planetary Science Letters* **271**, 123-134

HARFORD, C. L., PRINGLE, M. S., SPARKS, R. S. J. & YOUNG, S. R. 2002. The volcanic evolution of Montserrat using 40Ar/39Ar geochronology. *In*: Druitt, T.H. & Kokelaar, B.P. (eds). *The eruption of the Soufrière Hills Volcano, Montserrat from 1995 to 1999. Geological Society, London, Memoir* **21**, pp. 93-113.

HUMPHREYS, M., CHRISTOPHER, T. & HARDS, V. 2009a. Microlite transfer by disaggregation of mafic inclusions following magma mixing at Soufrière Hills volcano, Montserrat. *Contributions to Mineralogy and Petrology* **157**, 609-624. Doi: 10.1007/s00410-008-0356-3.

HUMPHREYS, M. C. S., EDMONDS, M., CHRISTOPHER, T. & HARDS, V. 2010. Magma hybridisation and diffusive exchange recorded in heterogeneous glasses from Soufrière Hills Volcano, Montserrat. *Geophys. Res. Lett.* **37**, L00E06. doi:10.1029/2009GL041926.

HUMPHREYS, M.C.S., EDMONDS, M., PLAIL, M., BARCLAY, J., PARKES, D., CHRISTOPHER, T. 2012. A new method to quantify the real supply of mafic components to a hybrid andesite. *Contributions to Mineralogy and Petrology.* In press. DOI: 10.1007/s00410-012-0805-x.

LEAKE, B. A., WOOLLEY, A. R., ARPS, C. E. S., BIRCH, W. D., GILBERT, M. C., GRICE, J. D., HAWTHORNE, F. C., KATO, A., KISCH, H. J., KRIVOVICHEV, V. G., LINTHOUT, K., LAIRD, J., MANDARINO, J. A., MARESCH, W. V., NICKEL, E. H., ROCK, N. M. S., SCHUMACHER, J. C., SMITH, D. C., C.N, S. N., UNGARETTI, L., WHITTAKER, E. J. W. & YOUHZI, G. 1997. Nomenclature of Amphiboles: Report of the Subcommitte on Amphiboles of the International Mineralogical Association, commission on new minerals and mineral names. *The Canadian Mineralogist* **35**, 219-246.

828 MANN, C.K. 2010. Magma chamber dynamics at Soufrière Hills Volcano, Montserrat.
829 PhD thesis, McGill University
830 MARTIN, V. M., HOLNESS, M. B. & PYLE, D. M. 2006a. Textural analysis of magmatic
831 enclaves from the Kameni Islands, Santorini, Greece. *Journal of Volcanology and*
832 *Geothermal Research* **154**, 89-102.
833 MARTIN, V. M., PYLE, D. M. & HOLNESS, M. B. 2006b. The role of crystal frameworks
834 in the preservation of enclaves during magma mixing. *Earth and Planetary Science*
835 *Letters* **248**, 787-799.
836 MATTIOLI, G. S. & HERD, R. 2003. Correlation of cyclic surface deformation recorded
837 by GPS geodesy with surface magma flux at Soufrière Hills Volcano, Montserrat.
838 *Seismol. Res. Lett* **74**, 230.
839 MURPHY, M. D., SPARKS, R. S. J., BARCLAY, J., CARROLL, M. R. & BREWER, T. S.
840 2000. Remobilization of Andesite Magma by Intrusion of Mafic Magma at the Soufrière
841 Hills Volcano, Montserrat, West Indies. *Journal of Petrology* **41**, 21 - 42.
842 MURPHY, M. D., SPARKS, R. S. J., BARCLAY, J., CARROLL, M. R., LEJEUNE, A. M.,
843 BREWER, T. S., MACDONALD, R., BLACK, S. & YOUNG, S. 1998. The Role of Magma
844 Mixing in Triggering the Current Eruption at the Soufrière Hills Volcano, Montserrat,
845 West Indies. *Geophys. Res. Lett.* **25**.
846 NAKAGAWA, M., WADA, K. & WOOD, C. P. 2002. Mixed Magmas, Mush Chambers
847 and Eruption Triggers: Evidence from Zoned Clinopyroxene Phenocrysts in Andesitic
848 Scoria from the 1995 Eruptions of Ruapehu Volcano, New Zealand. *Journal of Petrology*
849 **43**, 2279-2303.
850 NELSON, S. T. & MONTANA, A. 1992. Sieve-textured plagioclase in volcanic rocks
851 produced by rapid decompression. *American Mineralogist* **77**, 1242-1249.
852 PALLISTER, J. S., HOBLITT, R. P. & REYES, A. G. 1992. A basalt trigger for the 1991
853 eruptions of Pinatubo volcano? *Nature* **356**, 426-428.
854 PLECHOV, P.Y., TSAI, A.E., SHCHERBAKOV, D., DIRKSEN, O.V. 2008. Opacitization
855 conditions of hornblende in Bezymyannyi Volcano andesites (March 30 1956 eruption)
856 *Petrology* **16**, 19-35
857 RIDOLFI, F. & RENZULLI, A. 2011. Calcic amphiboles in calc-alkaline and alkaline
858 magmas: thermobarometric and chemometric empirical equations valid up to 1,130_C
859 and 2.2 GPa. *Contributions to Mineralogy and Petrology* **163**, 877-895.

RUPRECHT, P. & WÖRNER, G. 2007. Variable regimes in magma systems documented in plagioclase zoning patterns: El Misti stratovolcano and Andahua monogenetic cones. *Journal of Volcanology and Geothermal Research* **165**, 142-162.

RUTHERFORD, M. J. & DEVINE, J. D. 2003. Magmatic Conditions and Magma Ascent as Indicated by Hornblende Phase Equilibria and Reactions in the 1995-2002 Soufrière Hills Magma. *J. Petrology* **44**, 1433-1453.

SINGER, B. S., DUNGAN, M. A. & LAYNE, G. D. 1995. Textures and Sr, Ba, Mg, Fe, K and Ti compositional profiles in volcanic plagioclase clues to the dynamics of calc-alkaline magma chambers. *American Mineralogist* **80**, 776-798.

SNYDER, D., CRAMBES, C., TAIT, S. & WIEBE, R. A. 1997. Magma Mingling in Dikes and Sills. *The Journal of Geology* **105**, 75-86.

SPARKS, R. S. J. & MARSHALL, L. A. 1986. Thermal and mechanical constraints on mixing between mafic and silicic magmas. *Journal of Volcanology and Geothermal Research* **29**, 99-124.

SPARKS, R.S.J., MURPHY, M.D., LEJEUNE, A.M., WATTS, R.B., BARCLAY, J. & YOUNG, S.R. 2000. Control on the emplacement of the andesite lava dome of the Soufrière Hills volcano, Montserrat by degassing-induced crystallization. *Terra Nova* **12**, 14-20.

STINTON, A.J., COLE, P.D., ODBERT, H.M., *et al.* (this volume) Geomorphic changes at the Soufrière Hills Volcano, Montserrat, during a short intensive episode of dome growth: 4 October 2009 - 11 February 2010. *Geol. soc memoir*

TEPLEY, F. J., DAVIDSON, J. P. & CLYNNE, M. A. 1999. Magmatic Interactions as Recorded in Plagioclase Phenocrysts of Chaos Crags, Lassen Volcanic Center, California. *Journal of Petrology* **40**, 787-806.

THOMAS, N. & TAIT, S. R. 1997. The dimensions of magmatic inclusions as a constraint on the physical mechanism of mixing. *Journal of Volcanology and Geothermal Research* **75**, 167-178.

TURNBULL, R., WEAVER, S., TULLOCH, A., COLE, J., HANDLER, M. & IRELAND, T. 2010. Field and Geochemical Constraints on Mafic–Felsic Interactions, and Processes in High-level Arc Magma Chambers: an Example from the Halfmoon Pluton, New Zealand. *Journal of Petrology* **51**, 1477-1505.

WADGE, G., VOIGHT, B., SPARKS, R.S.J., COLE, P., LOUGHLIN, S.C. (this volume) An overview of the Soufrière Hills Volcano from 2000 -2010. *Geol. soc. memoir*

WIEBE, R. A. 1993. The Pleasant Bay Layered Gabbro—Diorite, Coastal Maine: Ponding and Crystallization of Basaltic Injections into a Silicic Magma Chamber. *Journal of Petrology* **34**, 461-489.

WIEBE, R. A., SMITH, D., STURM, M., KING, E. M. & SECKLER, M. S. 1997. Enclaves in the Cadillac Mountain Granite (Coastal Maine): Samples of Hybrid Magma from the Base of the Chamber. *Journal of Petrology* **38**, 393-423.

ZELLMER, G. F. HAWKESWORTH., C. J. SPARKS, R. S. J. THOMAS, L. E. HARFORD, C. L. BREWER, T. S. LOUGHLIN, S. C. 2003. Geochemical Evolution of the Soufrière Hills Volcano, Montserrat, Lesser Antilles Volcanic Arc. *Journal of Petrology* **44**, 1349 -1374.

Figures

Figure 1: (a) A representative image of an andesitic block from Feb 11 2010 dome collapse (scale: 10 cm with 2 cm intervals). (b) is an image of the net employed during point counting of mafic enclaves. Net is $1m^2$, string is spaced at 10 cm intervals, with 2 cm tick marks. (c) Image of type A and B enclaves seen in the field. Note distinct colour difference and the clearly distinct margins in A as opposed to B (d) shows typical diktytaxitic framework observed in mafic enclaves with inherited phenocrysts of plagioclase (plag), amphibole (amp) and orthopyroxene (opx).

Figure 2: Frequency size distribution of measured enclave apparent diameters from andesitic blocks used to evaluate mafic enclave abundance in Table 2.

Figure 3: Inherited plagioclase phenocrysts overgrowth rim width (measured distance from crystal edge to sieve-texture) versus sieve-texture width. Increasing rim width is correlated with sieve-texture width. Note that where sieve-texture width is greater than 1000μm the sieve-texture pervades through to the crystal core.

Figure 4: All images are representative of type A enclaves. (a) Large type A enclave from Feb 11 2010 dome collapse deposit. Darkening of andesite around the enclave is an artefact of water spray used to clean the outcrop (scale: 10 cm with 2 cm intervals) (b) Photomicrograph of a type A chilled margin shown by a reduction in framework crystal size; andesite is on the left and mafic enclave on the right (c) Photomicrograph of type A framework crystals, Fe-Ti oxides (ox) (d) BSE image of framework plagioclase with sieve-

texture developing in the interior of the crystal. (e) BSE image of a clinopyroxene reaction rim developing on a high-Al amphibole microphenocryst.

Figure 5: Vesicle size distribution of measured type A and B enclaves.

Figure 6: Total inherited phenocryst modal proportions by enclave type against SiO_2 composition. A total of 16 enclaves were used and we observe that enclave types A and B plot in two distinct fields. Details of the inherited phenocryst type proportions counting are shown in Table 4.

Figure 7: Groundmass glass compositions of enclave types from electron probe analyses. (a) SiO_2 vs. K_2O. Type Ci (interior of portion of composite enclave), Type Ce (exterior portion) (b) FeO*tot vs. MgO.

Figure 8: (a) to (d) are representative of type B enclaves; (e) to (f) are representative of type C. (a) Type B enclaves sized from 2 cm to >10 cm in a single andesite block from Feb 11 2010 dome collapse deposit (scale: 10 cm with 2 cm intervals) (b) Photomicrograph of a diffuse margin between the host andesite and type B enclave. (c) Photomicrograph of small orthopyroxene microlites growing outwards from vesicle walls in pools of glass. Concentrations of glass are often associated with larger coalesced vesicles. (d) BSE image of a type B groundmass. Note zoning of opx crystal to cpx from core to rim. (e) Hand specimen image of the type C enclave used for this study (MT08) with an inner mafic portion and a hybrid mafic exterior portion (f) Photomicrograph of the margin between the inner and outer enclave portions The interior to the right of the margin contains more glass and high-Al amphibole microphenocrysts than the exterior portion to the left of the margin.

Figure 9: Comparison of XRF bulk geochemistry of mafic enclaves and host andesite across the first five phases of extrusive activity. Open symbols are SHV andesite and closed symbols are mafic enclaves. Phase I (Murphy *et al*. 2000; Zellmer *et al*. 2003); Phase II (Mann 2010; Zellmer *et al*. 2003); Phase III (Barclay *et al*. 2010; this study); Phases IV to V (this study)

Figure 10: Comparison of mafic enclave types A, B and C from Phase V using representative XRF bulk geochemistry data. Arrows indicate projected effect of adding equal proportions of inherited plagioclase and amphiboles phenocrysts to the least evolved mafic enclave bulk composition.

Figure 11: Simplified modelled effective viscosity of SHV host andesite and mafic enclaves against temperature. Melt viscosity was modelled using the method of Giordano *et al*. (2008) and effective viscosity using the Einstein-Roscoe relation. Andesite sample has 77 wt % SiO_2 40% crystals, 4% wt % H_2O. We use three enclave samples using measured bulk compositions, and assume modal inherited phenocryst proportions are mixed in prior to enclave formation. Type A (MT27) is the least evolved phase V sample with 49 wt % SiO_2, 8% inherited phenocryst volume, and 6 wt % H_2O. Type B end-members were modelled (1) 53 wt % SiO_2 and 16% inherited phenocrysts, 6 wt % H_2O (2) 58 wt % SiO_2, 24% inherited phenocrysts, and 6 wt % H_2O. We assume mafic magma temperatures of between 950-1100°C, and similar temperatures for Types A and B for the purposes of this model, H_2O contents from Edmonds *et al*. (this volume) and andesite temperatures from Barclay *et al*. (1998).

Figure 12: Proposed mingling model for Phase V from petrological, textural and geochemical analysis of mafic enclave types. (A) Type A enclaves form during intrusion of a mafic magma plume either at plume margins or from 'spray'. Collapse of plume as indicated by arrows is driven by both density and gravity contrasts, or by a reduction in the rate of mafic injection. Andesite derived phenocrysts and melt are engulfed by the intruding mafic magma forming a hybrid mafic magma, which ponds towards the magma chamber base, with perhaps denser material at the base. (B) Hybridised mafic magma derived from the collapse of a plume; hybridised as a result of localised mixing with the andesite is shown at the base of the chamber. At the hybrid mafic-andesite interface crystallisation results due to cooling of the hybrid mafic layer. Type B enclaves are derived from this layer either as the result of blobs of magma detaching from the layer or breakup of the layer. Mafic material may also continue to pond at the base of the chamber beneath the mafic hybrid due to quasi-continuous input of mafic material. (C) Type C enclaves may be the result of multiple injections of mafic magma. Blobs of mafic magma may detach from the intruding magma as it intrudes through the mafic hybrid, mingling with the hybrid magma. Composite enclave textures are only likely to form where viscosity and temperature contrast is greatest between the mafic and mafic hybrid *i.e.* close to the mafic-silicic interface.


a


b

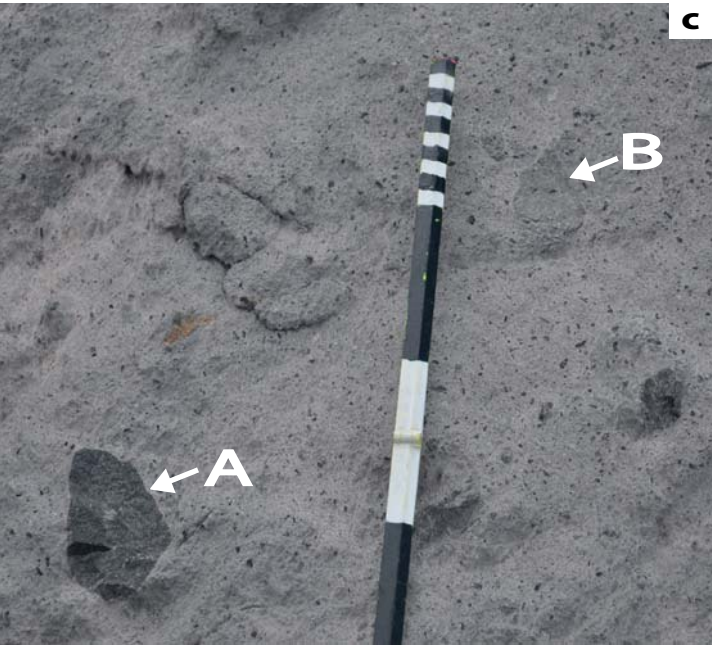
c
B
A

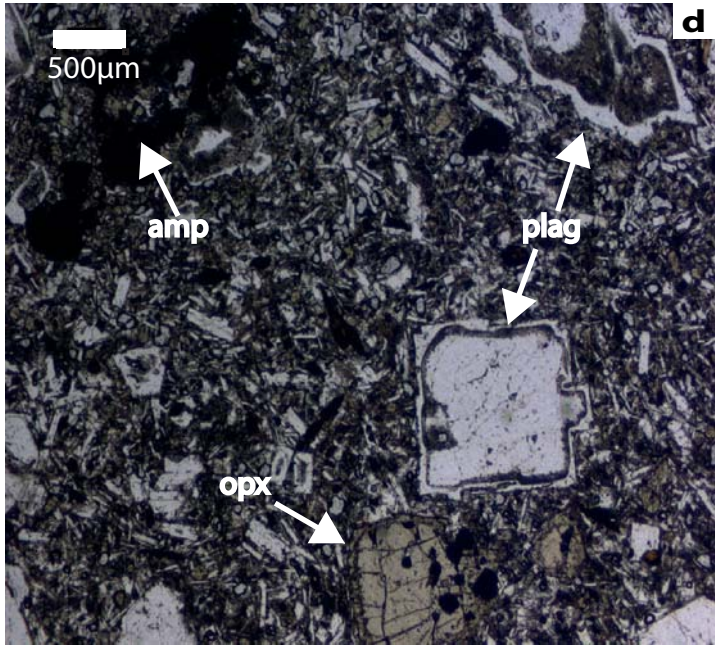
d
500µm
amp
plag
opx

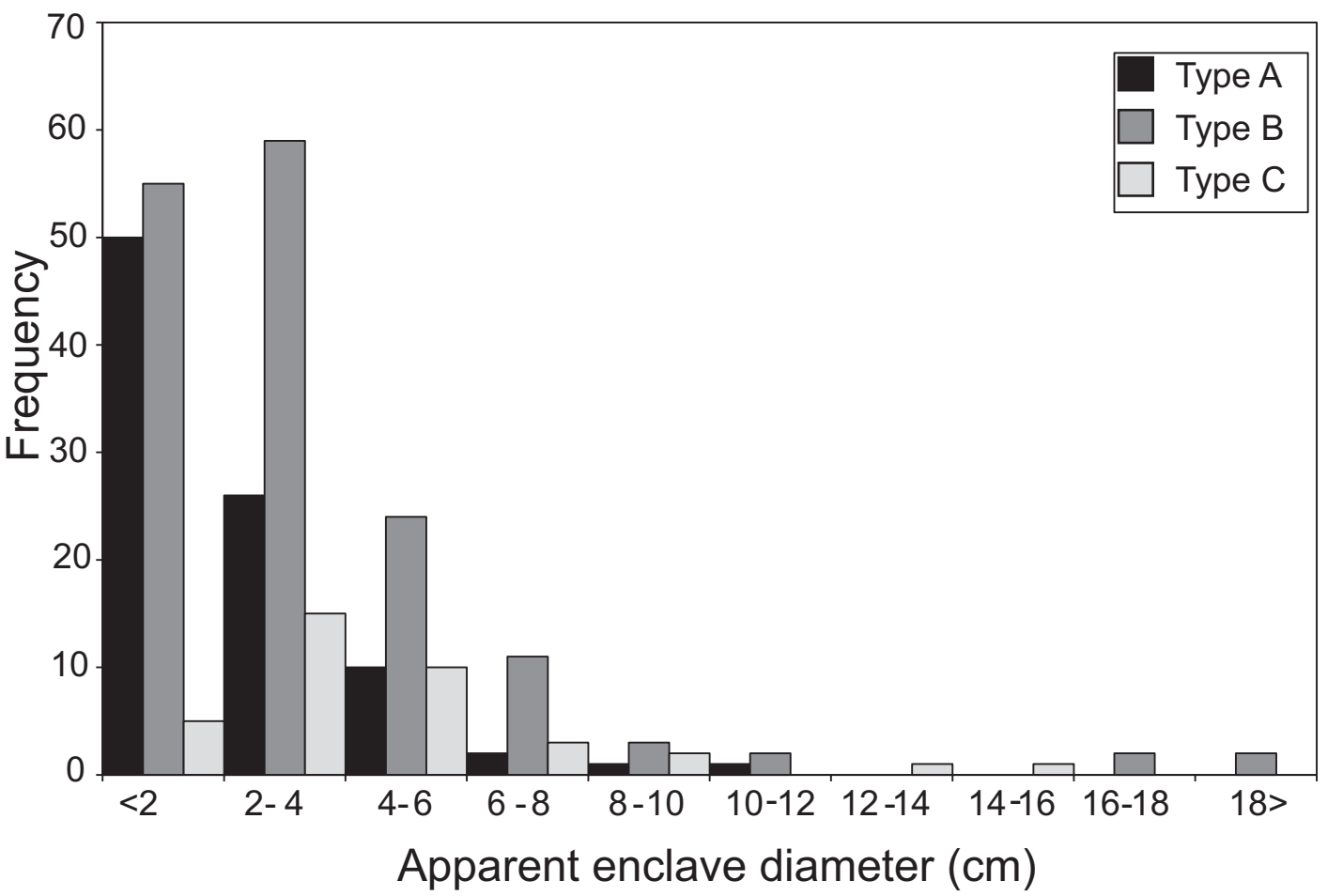
70
60
50
40
30
20
10
0
Frequency
Type A
Type B
Type C
<2
2- 4
4-6
6 -8
8 -10
10-12
12 -14
14-16
16-18
18>
Apparent enclave diameter (cm)

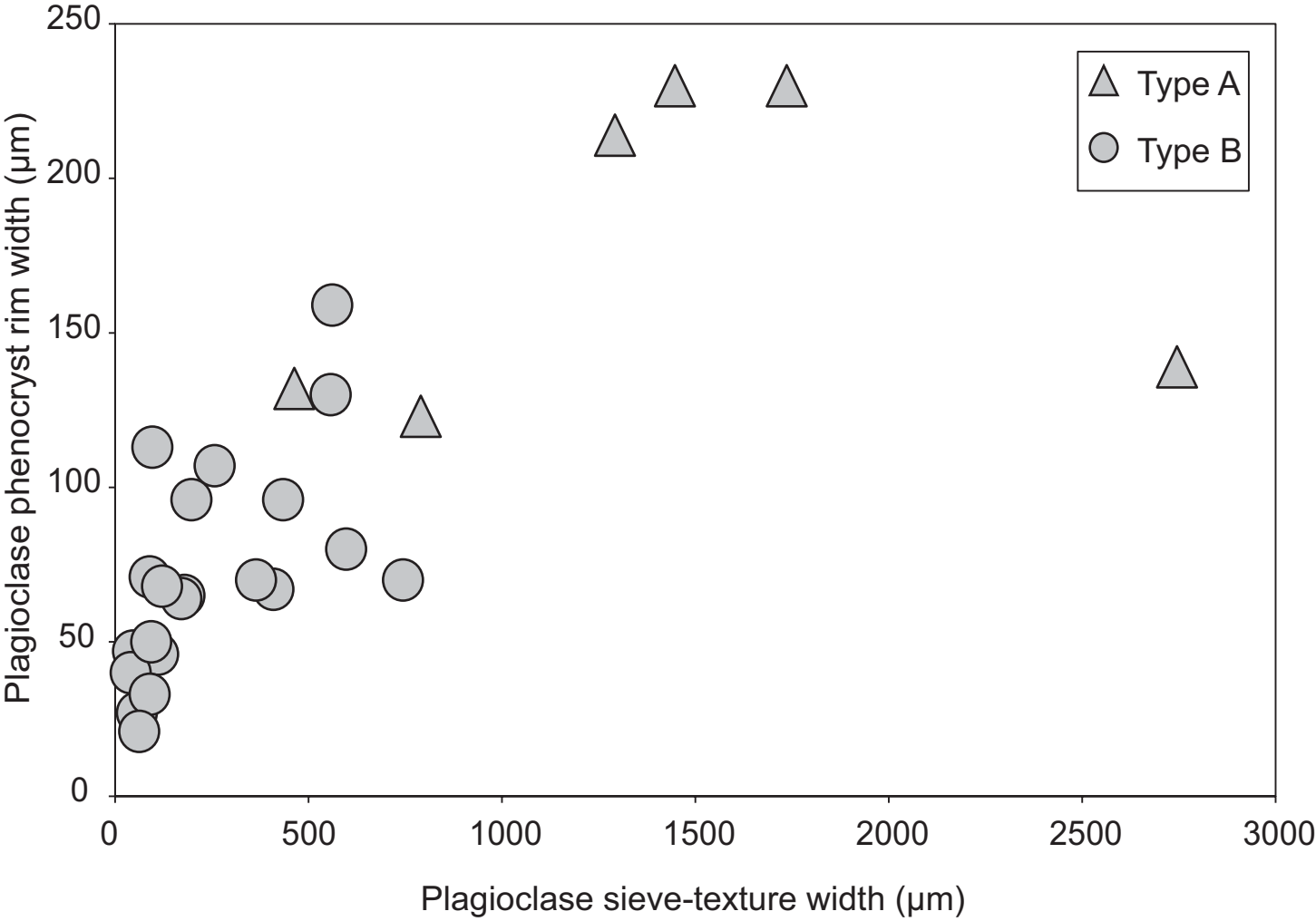
Type A
Type B
Plagioclase phenocryst rim width (μm)
Plagioclase sieve-texture width (μm)
0
50
100
150
200
250
0
500
1000
1500
2000
2500
3000


a

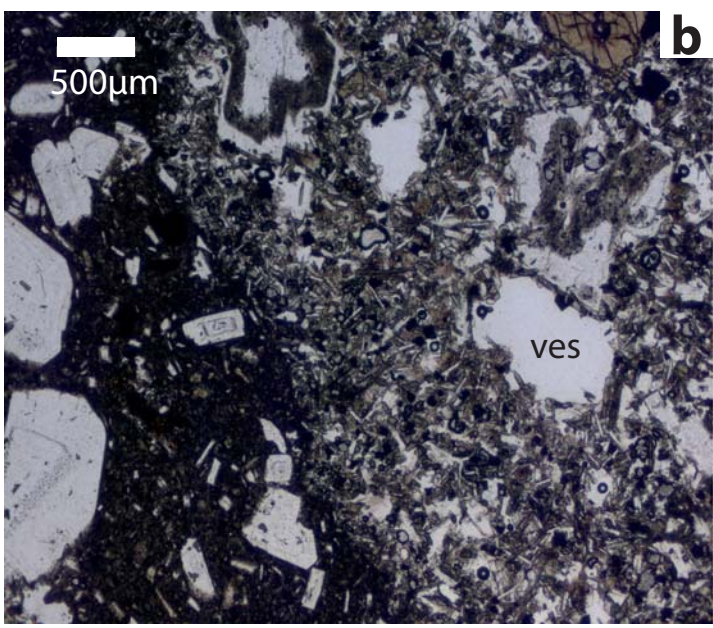
b
500µm
ves

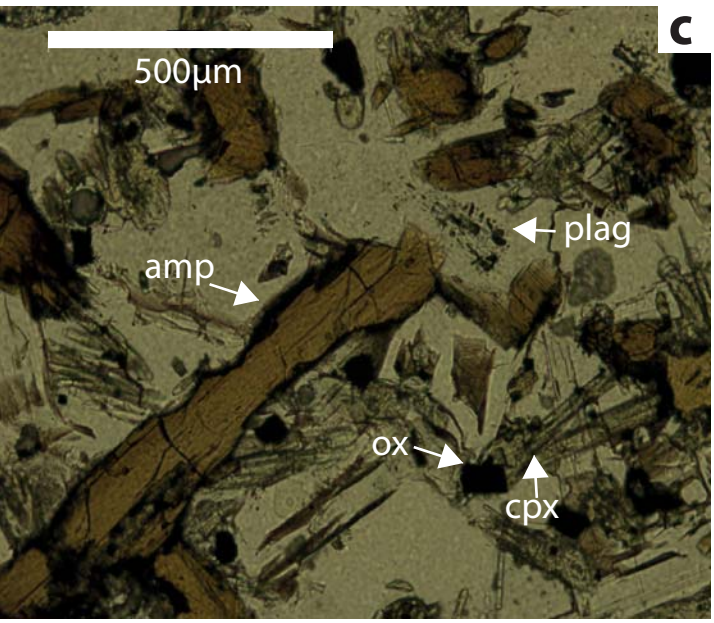
c
500µm
plag
amp
ox
cpx

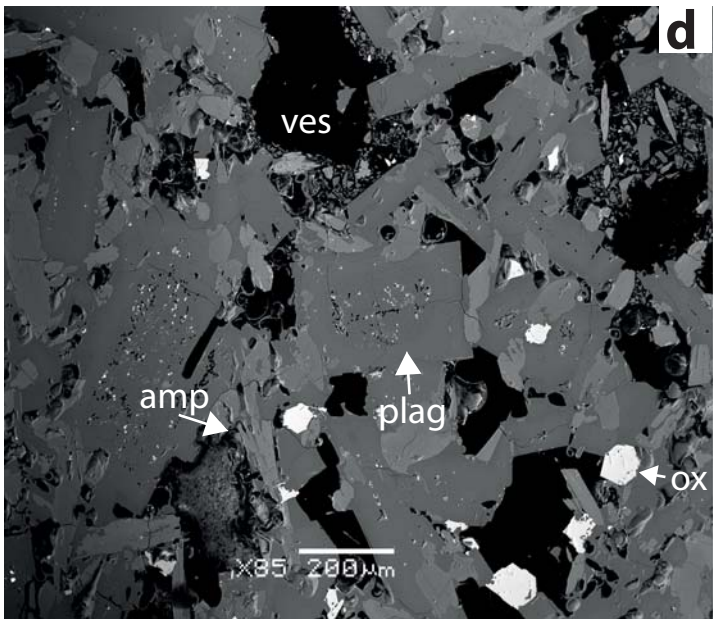
d
ves
amp
plag
ox
X85 200µm

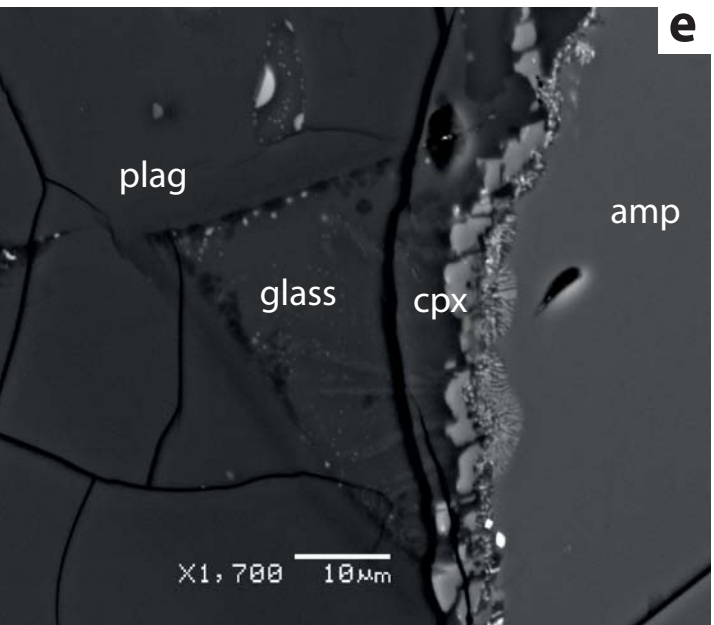
e
plag
amp
glass
cpx
X1,700 10µm

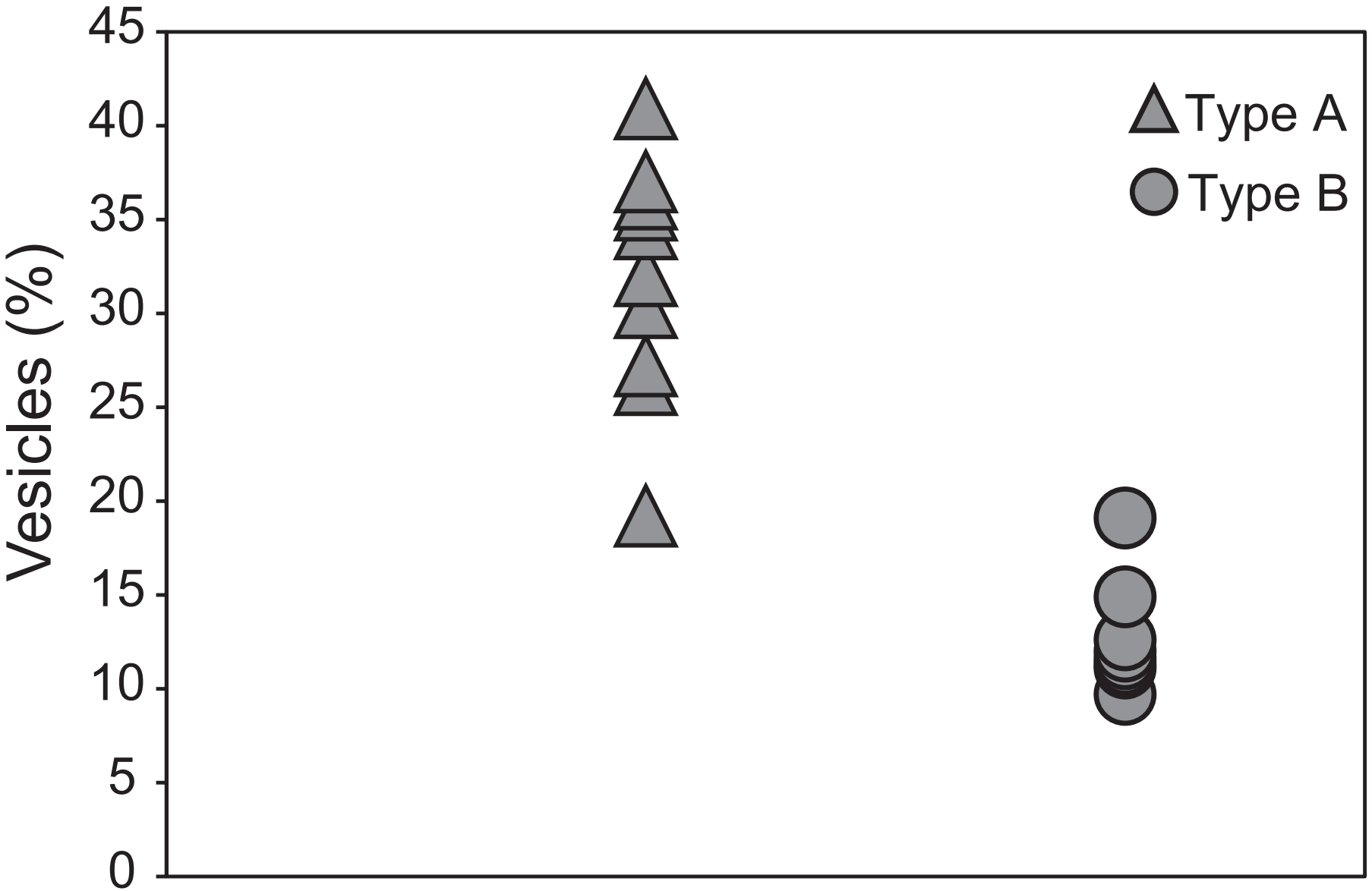
Vesicles (%)
45
40
35
30
25
20
15
10
5
0
Type A
Type B

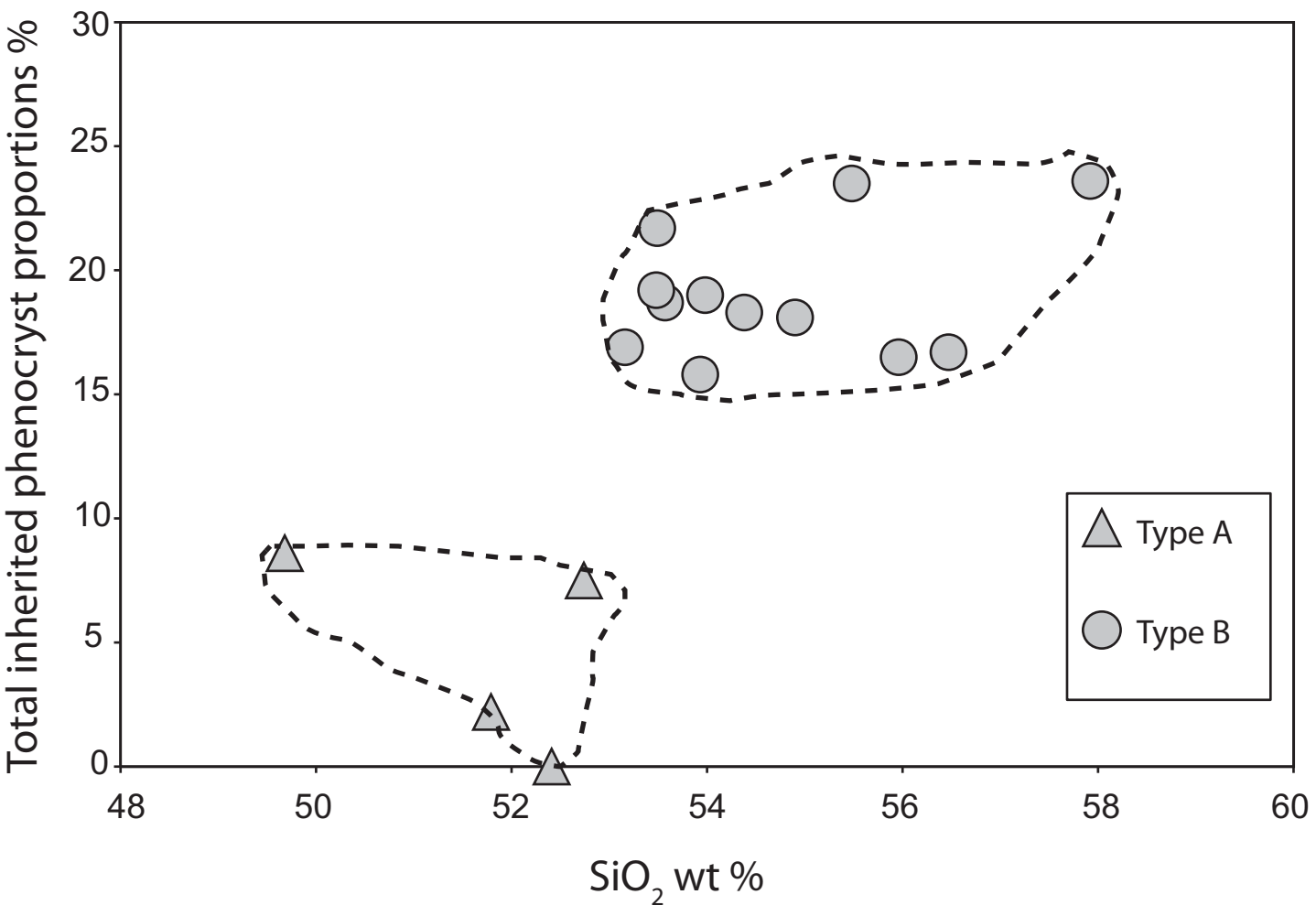
Total inherited phenocryst proportions %
30
25
20
15
10
5
0
48
50
52
54
56
58
60
SiO2 wt %
Type A
Type B

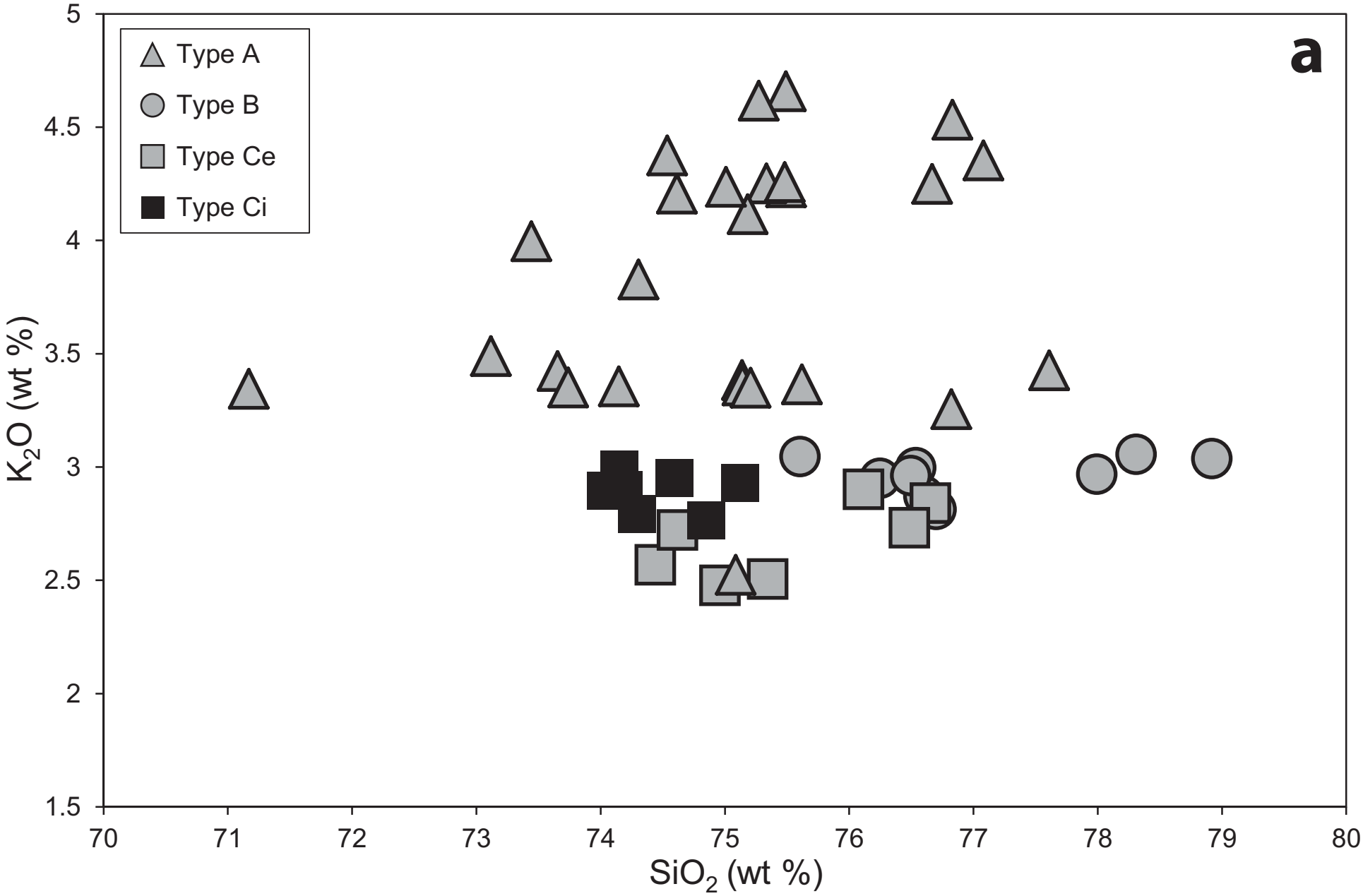
a
Type A
Type B
Type Ce
Type Ci
K_2O (wt %)
SiO_2 (wt %)
5
4.5
4
3.5
3
2.5
2
1.5
70
71
72
73
74
75
76
77
78
79
80

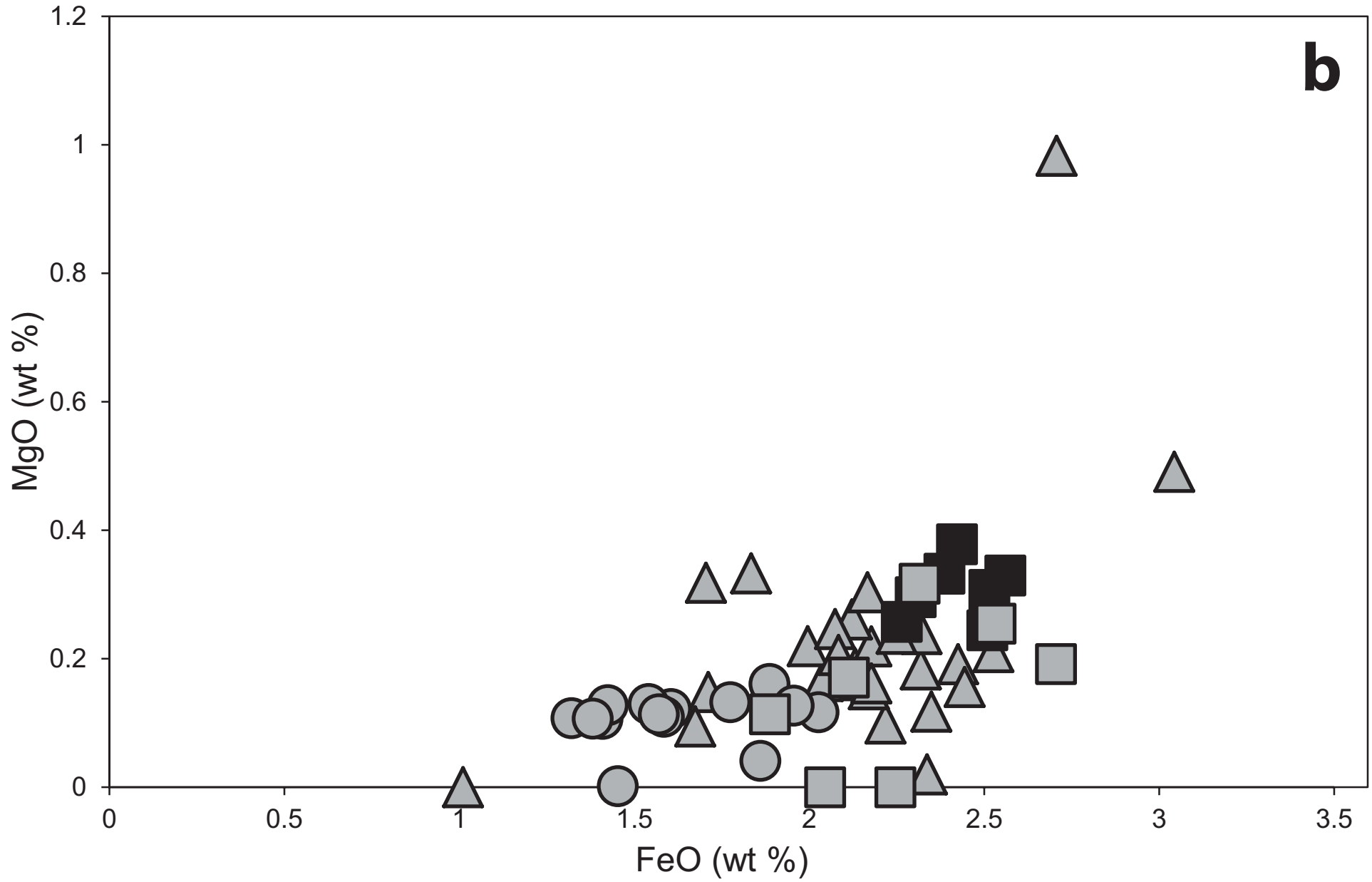
b
MgO (wt %)
FeO (wt %)
1.2
1
0.8
0.6
0.4
0.2
0
0
0.5
1
1.5
2
2.5
3
3.5

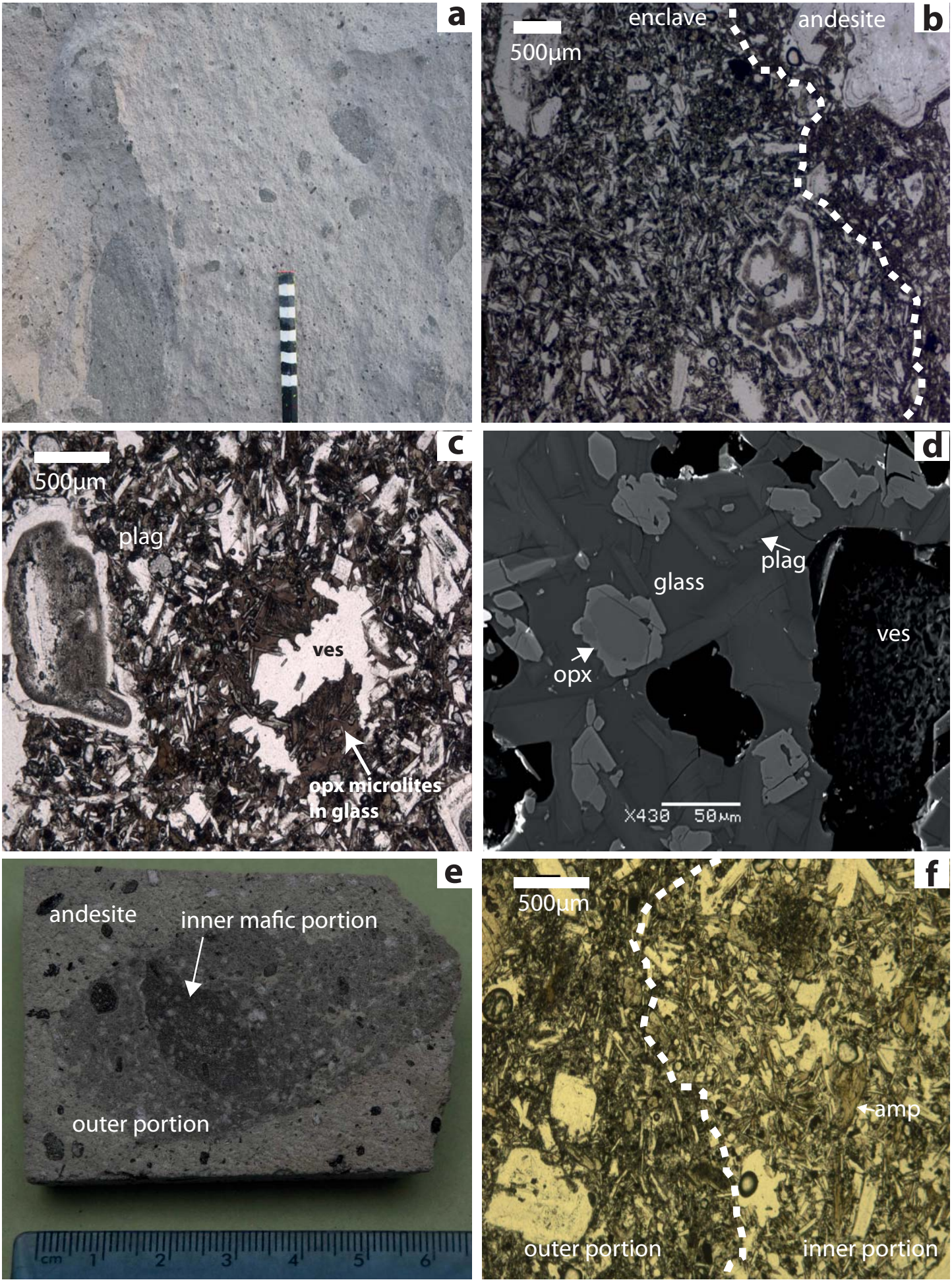
a
b
enclave
andesite
500µm
c
500µm
plag
ves
opx microlites
in glass
d
plag
glass
ves
opx
X430 50µm
e
andesite
inner mafic portion
outer portion
cm 1 2 3 4 5 6
f
500µm
amp
outer portion
inner portion

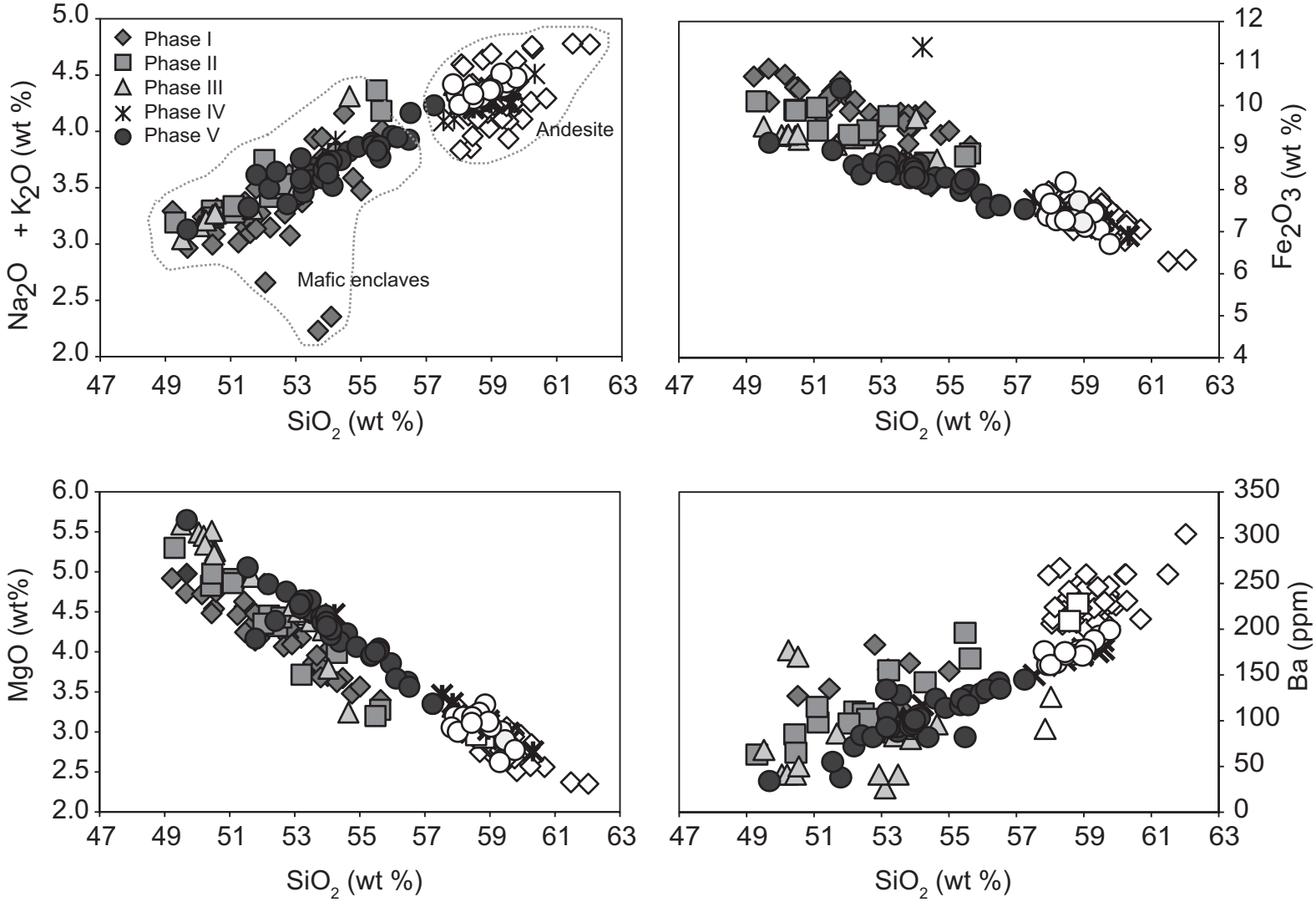
Phase I
Phase II
Phase III
Phase IV
Phase V
Andesite
Mafic enclaves
Na2O + K2O (wt %)
Fe2O3 (wt %)
MgO (wt%)
Ba (ppm)
SiO2 (wt %)
SiO2 (wt %)
SiO2 (wt %)
SiO2 (wt %)

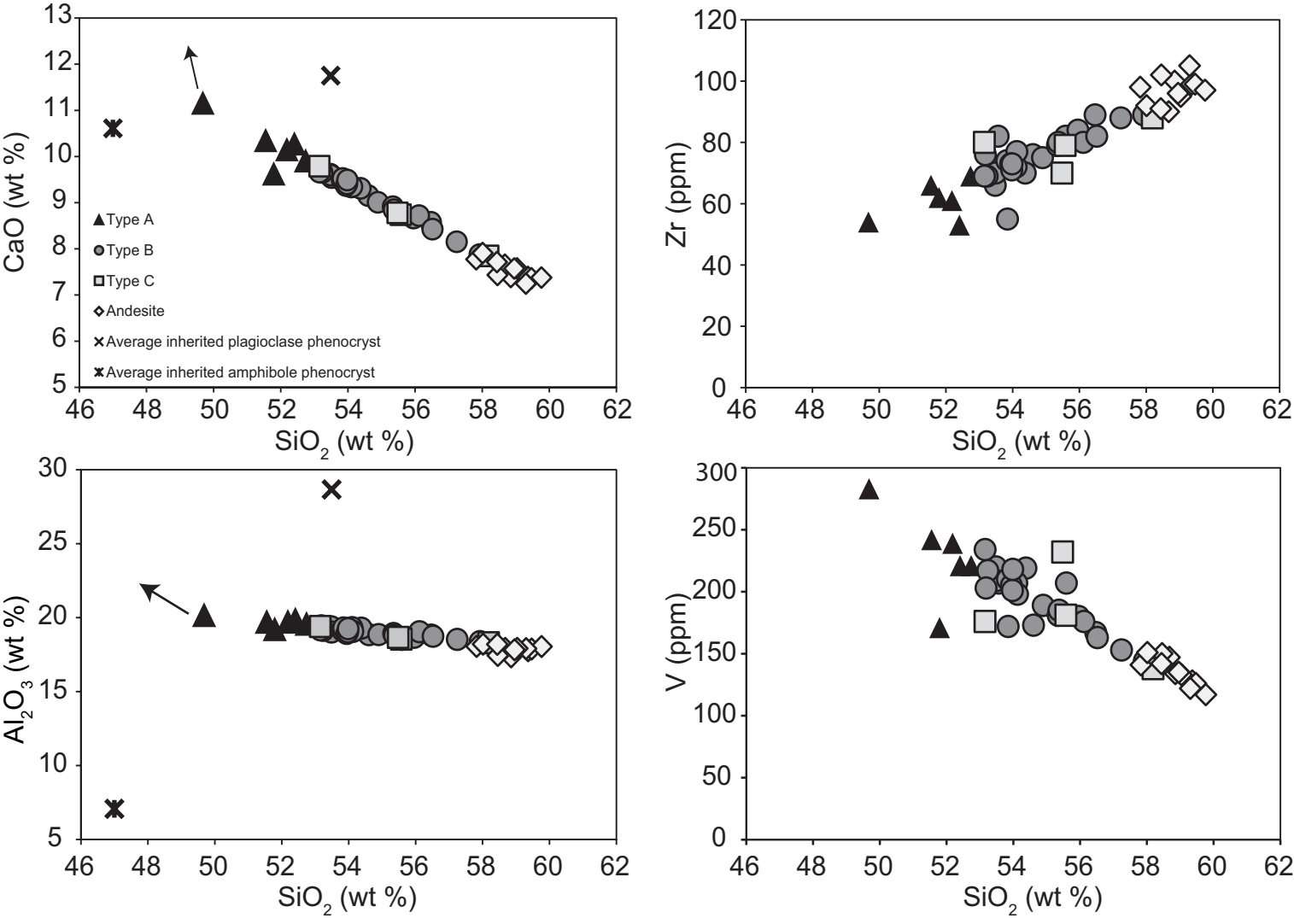
CaO (wt %)
SiO2 (wt %)
Type A
Type B
Type C
Andesite
Average inherited plagioclase phenocryst
Average inherited amphibole phenocryst
Zr (ppm)
SiO2 (wt %)
Al2O3 (wt %)
SiO2 (wt %)
V (ppm)
SiO2 (wt %)

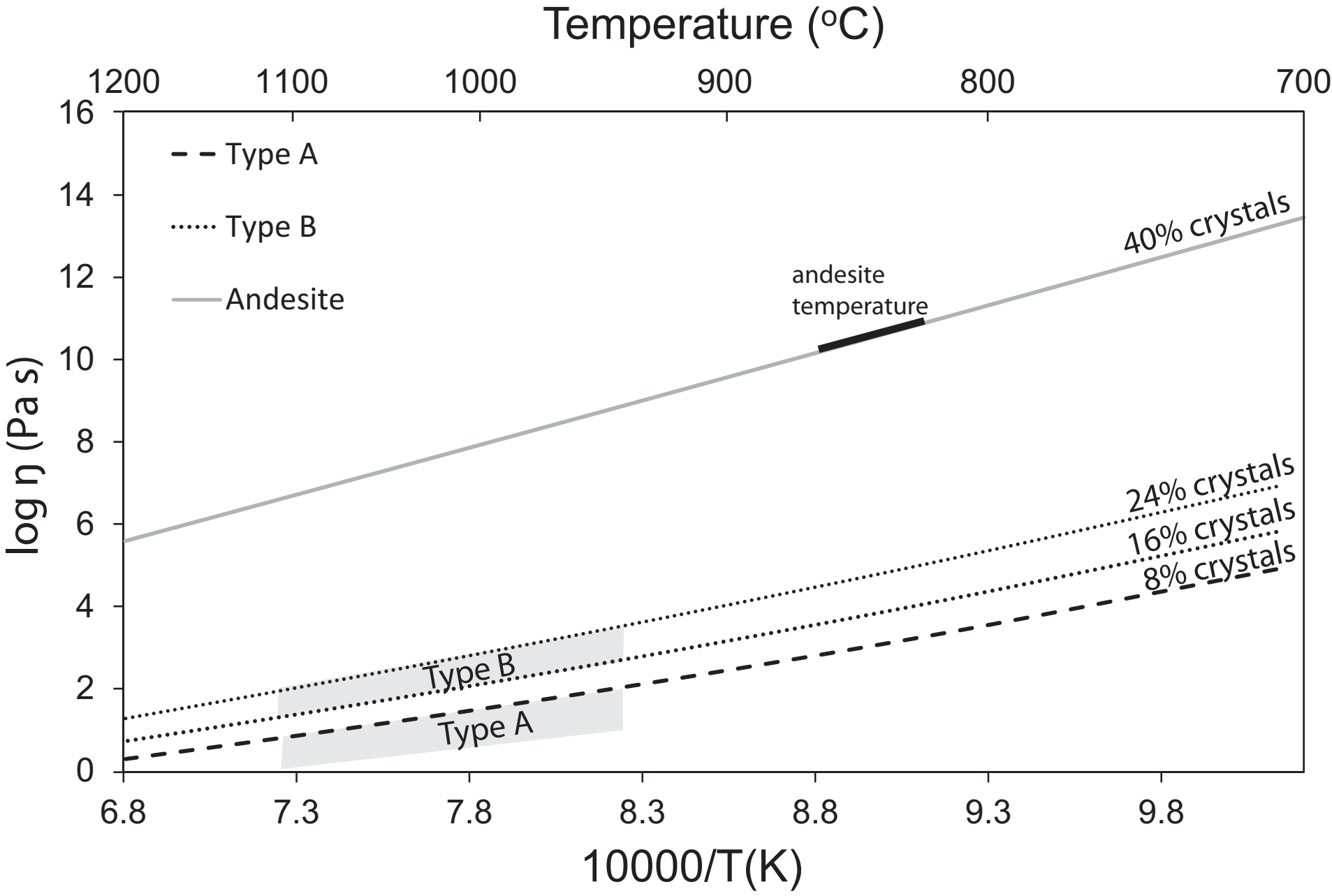
Temperature (°C)
1200
1100
1000
900
800
700
16
14
12
10
8
6
4
2
0
log η (Pa s)
Type A
Type B
Andesite
andesite
temperature
40% crystals
24% crystals
16% crystals
8% crystals
Type B
Type A
6.8
7.3
7.8
8.3
8.8
9.3
9.8
10000/T(K)

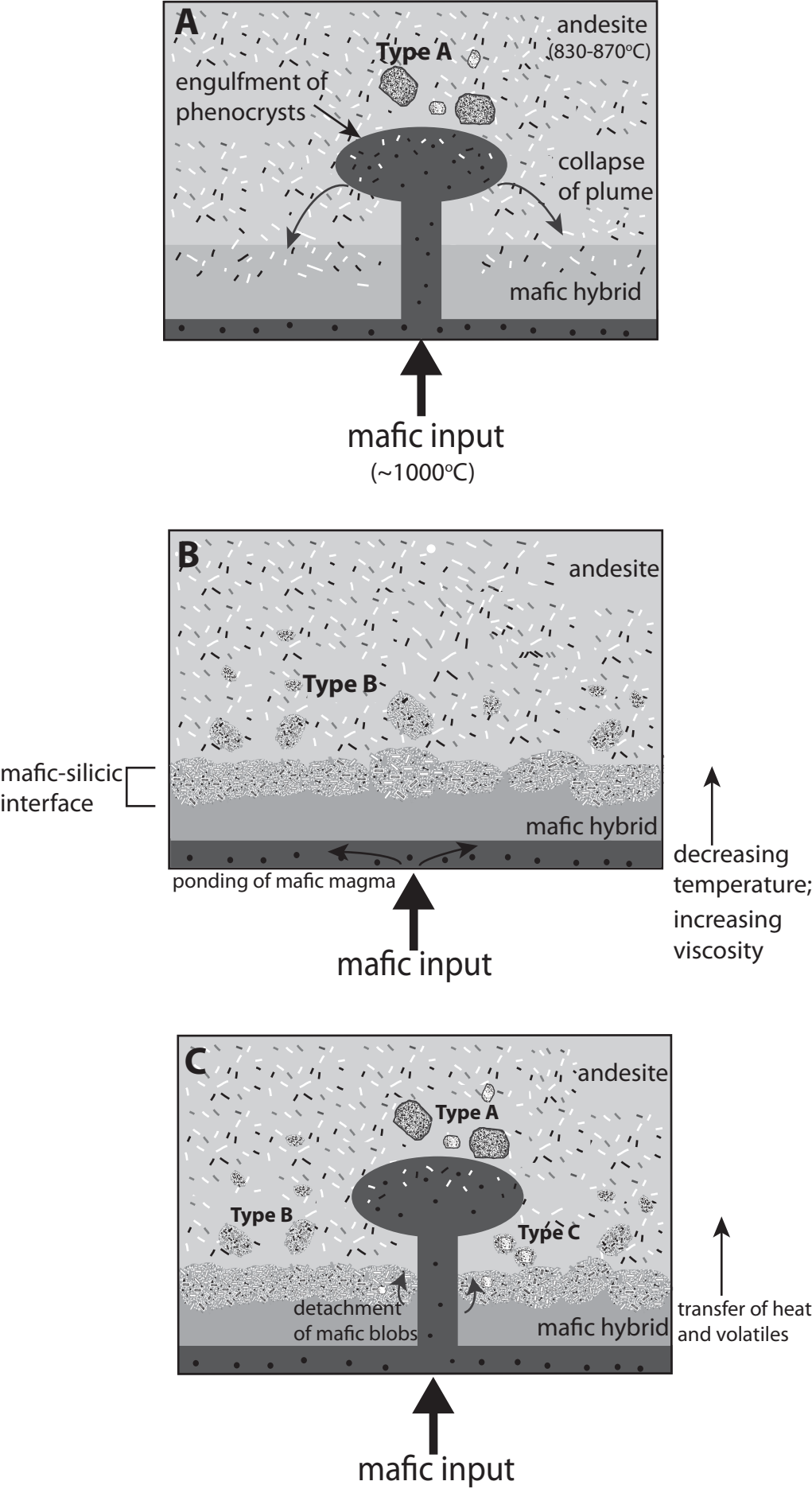
A
andesite
(830-870°C)
Type A
engulfment of
phenocrysts
collapse
of plume
mafic hybrid
mafic input
(~1000°C)
B
andesite
Type B
mafic-silicic
interface
mafic hybrid
ponding of mafic magma
mafic input
decreasing
temperature;
increasing
viscosity
C
andesite
Type A
Type B
Type C
detachment
of mafic blobs
mafic hybrid
transfer of heat
and volatiles
mafic input

Table 1: *Phase IV and V sample locations*

Sample no.	Location	GPS		Source	Date of emplacement
MVO1535	Lower Gages			Vulcanian explosion	03-Jan-2009
MT18-19, MVO1588, 1590,1591,1593	Aymers	583522	1846419	Pyroclastic flow	Jan-2010
MVO1566	Whites River	586880	1845330	Pyroclastic flow	Jan-2010
MVO1567	Bugby Hole	587400	1851433	Dome collapse	11-Feb-2010
MT20-MT37	Trants	589511	1852588	Dome collapse	11-Feb-2010
MT06-MT11	Streatham ridge	586695	1850599	Dome collapse	11-Feb-2010

Table 2. *Phase V mafic enclave proportional abundances*

Enclave type	**Block 1a***	**Block 1b***	**Block 2**	**Block 3**	**Block 4**	**Block 5**	**Block 6**	**Block 7**
Total points	1326	2550	2397	2397	2397	2397	2295	2601
Total enclaves points	47	155	137	196	125	115	67	126
Overall % of magmatic enclaves	3.54	6.08	5.72	8.18	5.21	4.80	2.92	4.84
Total number of enclaves measured	20	30	46	39	48	43	30	29
Type %								
A	0.00	30.32	13.14	4.59	27.20	27.83	46.27	29.37
B	100.00	60.65	77.37	80.61	54.40	31.30	52.24	52.38
C	0.00	9.03	9.49	14.80	18.40	40.87	1.49	18.25

*Block 1a and 1b is the same block, but two different faces were analysed

Table 3. *Summary of key features of enclave types A and B*

Type		Composition	Margin	Vesicularity	Framework crystals	Inherited phenocryst abundance	Inherited plagioclase phenocryst rim thickness
A	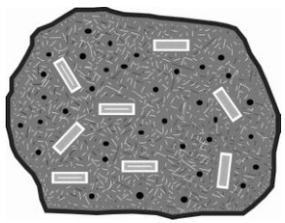	49-52 wt % SiO_2	Chilled	32% vol (mean)	High-Al amphibole present	<8% vol	132-230µm
B		53-57 wt % SiO_2	Unchilled to diffuse	13% vol (mean)	High-Al amphibole rare to absent	15-25% vol	27-113µm

Table 4. *Inherited phenocryst proportional abundances of phase V enclave types*

Inherited Phenocryst Type	***Type A (%)***	***Type B (%)***	***Type C: inner (%)***	***Type C: exterior (%)***
Plagioclase Type 1	*0*	*0.5-10.9*	*0*	*1.9*
Plagioclase Type 2	*0 -7*	*5 - 21*	*8.9*	*13*
Plagioclase Total	0 -7	8 - 21.2	8.9	14.9
Amphibole	0 - 2.9	1.2 - 8.5	3.3	6.7
Orthopyroxene	0 - 0.6	0.4 - 4.5	0	4.5
Total Range	**0-8**	**15.8 - 23.6**	**12.6**	**26.5**

Table 5. *Average compositions of selected minerals from mafic enclaves*

a) *Plagioclase framework (core)*

	Type A		**Type B**		**Type C Interior**		**Type C Exterior**	
		±1σ		±1σ		±1σ		±1σ
n	22		18		9		7	
SiO_2	47.02	1.80	49.90	1.89	45.82	0.94	48.86	1.15
TiO_2	0.02	0.01	0.03	0.01	0.02	0.01	0.03	0.01
Al_2O_3	33.12	1.29	31.17	1.13	32.84	0.79	30.62	1.01
FeO	0.61	0.09	0.68	0.06	0.59	0.04	0.70	0.06
SrO	0.03	0.03	0.04	0.01	0.01	0.06	0.03	0.04
MgO	0.08	0.02	0.07	0.02	0.07	0.03	0.08	0.02
CaO	17.12	1.36	14.68	1.35	17.02	0.68	14.89	0.94
Na_2O	1.82	0.80	3.28	0.82	1.76	0.39	3.01	0.52
K_2O	0.03	0.03	0.06	0.02	0.02	0.02	0.06	0.02
Total	99.82		99.93		98.12		98.34	
X_{An}	83.72	6.98	71.03	7.06	84.12	3.46	72.98	4.66

b) *Amphibole (core)*

	Type A		**Type B**		**Type C Interior**		**Type C Exterior**	
		±1σ		±1σ		±1σ		±1σ
n	18		10		5		na*	
SiO_2	41.27	0.74	41.88	2.20	40.21	0.43		
TiO_2	2.01	0.18	1.87	0.20	2.06	0.14		
Al_2O_3	14.77	1.10	13.81	2.59	14.97	0.40		
Cr_2O_3	0.01	0.01	0.01	0.01	0.00	0.02		
FeO	10.00	0.96	10.79	2.04	9.75	0.44		
MnO	0.12	0.03	0.18	0.14	0.11	0.05		
MgO	15.21	0.43	14.65	0.72	15.23	0.24		
CaO	11.96	0.21	11.66	0.42	11.96	0.19		
Na_2O	2.44	0.07	2.30	0.34	2.45	0.07		

K_2O	0.25	0.02	0.23	0.05	0.24	0.03
Cl	0.06	0.01	0.07	0.03	0.08	0.05
F	0.01	0.01	0.03	0.04	n.a.	
Total	98.09		100.25		99.88	

c) *Clinoyroxene*

	Type A		**Type B**		**Type C Interior**		**Type C Exterior**	
		±1σ		±1σ		±1σ		±1σ
n	9		9		5		8	
SiO_2	49.21	1.48	50.37	1.86	47.38	1.40	47.96	2.01
TiO_2	0.80	0.28	0.64	0.26	0.95	0.35	0.90	0.39
Al_2O_3	4.73	1.72	4.16	2.62	6.07	2.14	5.42	2.35
FeO	10.09	2.39	10.04	1.44	9.25	1.60	9.58	1.17
MnO	0.37	0.20	0.41	0.19	0.29	0.20	0.31	0.10
MgO	14.50	1.17	14.39	0.88	14.06	0.69	14.41	1.37
CaO	19.76	2.19	19.80	1.36	20.46	1.46	19.91	1.60
Na_2O	0.27	0.05	0.31	0.17	0.25	0.01	0.24	0.04
Total	99.75		100.87		98.76		98.82	

d) *Oxides*

	Type A		**Type B**		**Type C Interior**		**Type C Exterior**	
		±1σ		±1σ		±1σ		±1σ
n	10		17		na		6	
SiO_2	0.10	0.02	0.44	1.12			0.32	0.62
TiO_2	9.33	2.53	9.26	2.92			9.40	1.83
Al_2O_3	4.15	1.02	2.16	0.25			2.31	0.33
FeO	79.69	1.66	81.75	3.52			81.18	2.37
MnO	1.65	0.26	1.24	0.36			1.57	0.13
MgO	0.39	0.04	0.52	0.09			0.54	0.05

CaO	0.05	0.04	0.07	0.07			0.07	0.06
Total	95.38		95.46				95.41	

e) *Glass*

	Type A		**Type B**		**Type C Interior**		**Type C Exterior**	
		±1σ		±1σ		±1σ		±1σ
n	26		14		7		7	
SiO_2	75.05	1.38	77.05	1.29	74.46	0.40	75.52	0.90
TiO_2	0.63	0.14	0.39	0.05	0.64	0.10	0.51	0.05
Al_2O_3	12.21	0.65	11.50	0.43	12.07	0.27	11.75	0.28
FeO	2.20	0.30	1.63	0.23	2.42	0.11	2.26	0.28
MgO	0.23	0.18	0.11	0.04	0.31	0.05	0.15	0.12
MnO	0.05	0.06	0.06	0.04	0.06	0.04	0.12	0.07
CaO	1.18	0.41	1.01	0.32	1.42	0.12	1.52	0.14
Na_2O	4.16	0.47	3.61	0.16	4.00	0.17	3.91	0.11
K_2O	3.83	0.55	2.98	0.10	2.89	0.08	2.68	0.16
P_2O_5	0.13	0.11	0.11	0.25	0.22	0.08	0.22	0.09
Cl	0.35	0.17	0.46	0.11	0.52	0.08	0.47	0.08
Total	100.13		99.04		99.15		99.23	

*na: not available

Table 6. *Selected Phase IV and V XRF analyses*

Sample no:	**MVO1535d**	**MVO1535e**	**MT27**	**MT29**	**MVO1567d**	**MT35**	**MVO1566b**	**MT37b**	**MT09a**	**MT25b**	**MVO1593**
Eruption date	Jan-2009	Jan-2009	Feb-2010	Feb-2010	Feb-2010	Feb-2010	Dec-2009	Feb-2010	Feb-2010	Feb-2010	Feb-2010
Type			A	A	A	A	A	A	B	B	B
wt%											
SiO_2	53.85	53.47	49.54	51.60	51.50	52.01	51.96	52.84	56.24	57.22	54.72
TiO_2	0.97	0.77	0.88	0.80	0.82	0.80	0.79	0.80	0.67	0.66	0.73
Al_20_3	16.17	19.17	20.09	19.12	19.67	19.63	19.68	19.59	18.74	18.52	18.79
Fe_2O_3	11.31	8.61	9.09	10.37	8.93	8.55	8.29	8.64	7.60	7.53	8.26
MnO	0.24	0.17	0.16	0.23	0.17	0.16	0.21	0.17	0.16	0.17	0.18
MgO	4.44	4.54	5.63	4.15	5.05	4.83	4.35	4.76	3.61	3.35	4.05
CaO	8.21	9.6	11.12	9.58	10.33	10.11	10.18	9.92	8.54	8.15	8.98
Na_2O	3.29	3.11	2.71	3.18	2.78	2.93	3.16	2.74	3.24	3.49	3.24
K_2O	0.6	0.54	0.41	0.42	0.54	0.55	0.45	0.62	0.67	0.74	0.61
P_2O	0.24	0.11	0.09	0.18	0.11	0.10	0.08	0.11	0.12	0.13	0.12
LOI	†na	na	-0.11	-0.33	-0.28	-0.29	0.10	1.06	0.01	-0.36	0.08
Total	100.09	100.26	99.61	99.30	99.62	99.38	99.25	101.25	99.60	99.60	99.68
ppm											
Sc	25	22	35	19	29	27	24	25	19	15	21
V	214	206	283	171	242	239	221	221	167	153	193
Cu	bd	35	53	70	105	36	81	11	bd	bd	11
Zn	92	61	60	80	61	64	62	61	63	60	64
Rb	12	10	*bd	10	13	10	bd	15	14	16	12
Sr	233	267	273	299	270	272	274	264	261	262	268
Y	41	19	19	24	20	19	24	20	19	19	19
Zr	146	69	54	62	66	61	53	69	89	88	77
Ba	117	101	34	38	55	72	84	82	142	145	111
Ce	58	43	32	40	36	34	42	41	47	51	44

*bd: below detection; †na: not available

MVO1566e	**MT37a**	**MT11**	**MT08a**	**MT08b**
Feb-2010	Feb-2010	Feb-2010	Feb-2010	Feb-2010
B	B	B	C	C
54.14	56.61	55.30	52.88	55.58
0.74	0.66	0.74	0.78	0.73
19.20	18.77	18.43	19.30	18.55
8.10	7.64	8.21	8.38	8.22
0.16	0.17	0.18	0.17	0.18
4.11	3.57	4.02	4.57	4.01
9.27	8.44	8.73	9.74	8.74
3.13	3.39	3.10	3.02	3.23
0.60	0.78	0.65	0.54	0.64
0.11	0.13	0.12	0.11	0.13
0.12	-0.25	0.04	-0.06	-0.01
99.56	100.00	99.52	99.66	99.43
21	17	23	27	20
207	163	207	232	185
25	bd	bd	bd	bd
62	63	69	66	66
11	19	14	11	13
270	262	256	266	261
18	18	20	21	21
72	82	82	70	81
106	135	128	82	119
35	43	47	46	45